MCB
Journals.ASM.org

Nucleosome Spacing Generated by ISWI and CHD1 Remodelers Is Constant Regardless of Nucleosome Density

Corinna Lieleg,[a] Philip Ketterer,[b] Johannes Nuebler,[c] Johanna Ludwigsen,[a] Ulrich Gerland,[c] Hendrik Dietz,[b] Felix Mueller-Planitz,[a] Philipp Korber[a]

Adolf Butenandt Institute, Molecular Biology, University of Munich, Munich, Germany[a]; Walter Schottky Institute, Physics Department, Technical University of Munich, Garching near Munich, Germany[b]; Theory of Complex Biosystems, Physics Department, Technical University of Munich, Garching near Munich, Germany[c]

Arrays of regularly spaced nucleosomes are a hallmark of chromatin, but it remains unclear how they are generated. Recent genome-wide studies, *in vitro* and *in vivo*, showed constant nucleosome spacing even if the histone concentration was experimentally reduced. This counters the long-held assumption that nucleosome density determines spacing and calls for factors keeping spacing constant regardless of nucleosome density. We call this a clamping activity. Here, we show in a purified system that ISWI- and CHD1-type nucleosome remodelers have a clamping activity such that they not only generate regularly spaced nucleosome arrays but also generate constant spacing regardless of nucleosome density. This points to a functionally attractive nucleosome interaction that could be mediated either directly by nucleosome-nucleosome contacts or indirectly through the remodelers. Mutant *Drosophila melanogaster* ISWI without the HAND-SANT-SLIDE (HSS) domain had no detectable spacing activity even though it is known to remodel and slide nucleosomes. This suggests that the role of ISWI remodelers in generating constant spacing is not just to mediate nucleosome sliding; they actively contribute to the attractive interaction. Additional factors are necessary to set physiological spacing in absolute terms.

It is one of the earliest observations in molecular chromatin research that limited endonuclease digests of chromatin, for example, by micrococcal nuclease (MNase), generate quantized DNA fragment lengths. These are visualized as "MNase ladders" in agarose gel electrophoresis. The interpretation that such ladders originate from a regular array of repeating chromatin units, which restrict nuclease accessibility along DNA, together with electron microscopy evidence, led to the discovery that the nucleosome is the repeating unit of chromatin (1). A nucleosome consists of a core particle, where 147 bp are wrapped in ~1.7 turns around an octamer of basic histone proteins, and a stretch of linker DNA that connects core particles. Whereas the core particles are highly conserved between species, the linker DNA length varies considerably among species and even among cell types of the same species. The linker length typically ranges from 7 to ~50 bp but can exceed 100 bp (2). Recent genome-wide nucleosome mapping highlighted again pervasive regular nucleosomal arrays with species-specific nucleosome repeat lengths (3–8) and revealed further that such arrays are often aligned at biological features like transcription start sites (TSSs) (3) or replication origins (9, 10).

Array regularity may be important for higher-order packing of chromatin fibers (11–14), especially in heterochromatin (15). Recently, impaired genic arrays were correlated with increased cryptic transcription (16–19), arguing for their importance in suppressing the activity of cryptic promoter-like elements.

Even though regular nucleosomal arrays are pervasive, conserved, and functionally important, our understanding of how they are generated is rather limited. Nucleosome remodeling enzymes of the ISWI and CHD1 types (20) were implicated in this process (16–19, 21–25). These enzymes use ATP hydrolysis to mobilize nucleosomes along DNA ("nucleosome sliding") (26, 27). In some cases, so-called *in vitro* "spacing assays" guided their initial isolation from cell extracts (23–25). Such assays monitor the conversion of polynucleosomes with rather irregular linker lengths into evenly spaced regular arrays, especially with near-physiological repeat lengths. Accordingly, such "spacing activity" is considered a hallmark of the ISWI- and CHD1-type remodeling enzymes.

Nonetheless, the mechanism by which ISWI and CHD1 enzymes generate nucleosomal arrays and which determines nucleosome repeat length is unknown. The ISWI spacing activity is currently best explained by a "linker length sensor mechanism" (28), whereby the remodeling activity is increasingly stimulated by increasing linker lengths. The remodeler samples both sides of the nucleosome and is more active on the nucleosome side with the longer linker DNA such that it slides the nucleosome preferentially toward the longer linker. This will iteratively shorten the longer linker and lengthen the shorter linker and thereby equalize linker lengths at steady state. The human remodeling complex ACF, consisting of the *Drosophila melanogaster* ISWI homolog SNF2h and a noncatalytic subunit, Acf1, distinguishes linker lengths up to 60 bp (28). Beyond this limit, remodeler-mediated sliding is expected to result in a one-dimensional random walk.

In this linker length sensor mechanism, the repeat length does not result primarily from the remodeler but from the nucleosome density, becoming shorter with increasing density. This concept is

Received 19 August 2014 **Returned for modification** 21 September 2014
Accepted 14 February 2015

Accepted manuscript posted online 2 March 2015

Citation Lieleg C, Ketterer P, Nuebler J, Ludwigsen J, Gerland U, Dietz H, Mueller-Planitz F, Korber P. 2015. Nucleosome spacing generated by ISWI and CHD1 remodelers is constant regardless of nucleosome density. Mol Cell Biol 35:1588–1605. doi:10.1128/MCB.01070-14.

Address correspondence to Felix Mueller-Planitz, felix.mueller-planitz@med.uni-muenchen.de, or Philipp Korber, pkorber@lmu.de.

doi:10.1128/MCB.01070-14

akin to the classical model of statistical nucleosome positioning (29, 30). In this model, nucleosomes are modeled as hard noninteracting spheres that move freely along DNA, like particles of a one-dimensional gas. If nucleosome movement is restricted at an insurmountable barrier, they will form regular and barrier-aligned arrays merely due to their statistical movement, resulting in linker lengths that are reciprocally related to nucleosome density.

However, statistical positioning and the concept of nucleosome density-dependent spacing were recently challenged by several independent genome-wide nucleosome mapping studies both *in vitro* (31) and *in vivo* (16, 32–35). In all cases, reduced nucleosome density did not lead to substantially wider spacing. As *in vitro* array formation in the context of a whole-cell extract was ATP dependent, it was proposed that remodelers actively pack nucleosomes together (31). These data were more consistent with a "protein ruler mechanism" derived from structural data for the *Saccharomyces cerevisiae* ISW1a remodeler in complex with nucleosomes (36), where linker length is suggested to result from simultaneous interactions of the remodeling complex with two neighboring nucleosomes. In particular, the HAND-SANT-SLIDE (HSS) domain of ISWI-type remodelers was suggested to be important for nucleosome spacing, e.g., as a "protein ruler" (36).

In the context of this recent controversy, we provide now *in vitro* evidence that ISWI- and CHD1-type remodelers generate constant nucleosome spacing despite variations in nucleosome density. Our results disfavor models in which linker length simply results from nucleosome density. Instead, we propose that such remodelers are actively involved in nucleosomes staying together and that this clamping activity may depend on the HSS domain for the *Drosophila* ISWI remodeler. Additional factors are required to set the physiological repeat length in absolute terms.

MATERIALS AND METHODS

DNA templates and SGD chromatin assembly. Plasmids were isolated from *Escherichia coli* using the PureYield Maxiprep system (Promega). pUC19-PHO8 contains ~3.5 kb of the *Saccharomyces cerevisiae PHO8* locus cloned into pUC19 via BamHI and PstI, is 6,168 bp long, and is described as "pUC19-PHO8-long" in reference 37. pUC19-GCY1 contains ~3.5 kb of the *S. cerevisiae GCY1* locus (PCR product using primers 5′-CAGTCGGATGGAGCTCACTTCTATTGGCTTAGGAGC-3′ and 5′-CACTGTGCATTTCTAGAACGACGAAGACGAGGATTAG-3′ and genomic DNA of strain BY4741 [EUROSCARF] as the template) cloned into pUC19 via SacI and XbaI. pUC19-PHO8 and pUC19-GCY1 were linearized with BamHI (NEB), which cleaves right at or 400 bp downstream of, respectively, the upstream border between prokaryotic and eukaryotic DNA. The complete plasmids were used as the template for salt gradient dialysis (SGD) reconstitution, and complete linearization was confirmed by agarose gel electrophoresis prior to chromatin assembly. Linearized pUC19-PHO8 and pUC19-GCY1 plasmids were assembled into chromatin with purified *D. melanogaster* embryo histone octamers (38) by SGD as previously described (39). The pUC19-601-25-mer plasmid (pFMP233) carrying a 25-mer of 197-bp repeats of Widom601 sequence (40) derivatives with a unique KpnI site within the 19th positioning sequence is a derivative of the gene-synthesized 13-mer nucleosomal array plasmid described in reference 41. The 25-mer was created by subcloning the 13-mer into pUC19 and extension at a unique AvaI site by a Widom601 12-mer isolated from a partial AvaI digest of repetitive Widom601 sequences of the same repeat length. DNA used for 25-mer nucleosomal array assembly was excised from this plasmid by digestion with EcoRI and XbaI, gel purified, and end labeled with a Li-Cor compatible dye via a Klenow fill-in reaction (0.2 g DNA/liter, 33 μM dUTP-DY776 [Dyomics catalog no. 776-34], 33 μM dATP [NEB] in NEB buffer 2, 0.5 U Klenow exo-/μg DNA [NEB] for 30 min at 26°C). After stopping the labeling reaction with a 25 mM final concentration of EDTA and purification (Wizard SV gel and PCR cleanup system; Promega), the fluorescently labeled 25-mer template was assembled into chromatin by SGD (39) with light protection to avoid dye bleaching.

Remodeling reactions. All remodeling reactions were performed at 26°C in 100 μl in 20 mM HEPES-KOH, pH 7.5, 80 mM KCl, 4 mM $MgCl_2$, 0.5 mM EGTA, 12% glycerol, 2.5 mM dithiothreitol (DTT), and 10 mM $(NH_4)_2SO_4$, and reaction mixtures contained 3 mM ATP or adenylyl-methylenediphosphonate (AMP-PCP) (Sigma-Aldrich) and an ATP-regenerating system (10 mM creatine phosphate [Sigma], 20 ng/μl creatine kinase [Roche Applied Science]). Remodeling was started by adding ISWI or ACF (both 30 nM if not indicated otherwise), $ISWI_{864::13aa}$ and $ISWI_{871::13aa}$ (both 60 nM), or Chd1 (150 nM if not indicated otherwise) to SGD chromatin (1 μg DNA assembled into chromatin). This corresponds to roughly stoichiometric amounts (within a factor of two to five depending on the assembly degree and remodeler) of remodelers to nucleosomes (about 80 and 40 nM nucleosomes for high and low assembly degree, respectively). For $ISWI_{26-648}$, higher concentrations (1 to 10 μM) were used to compensate for decreased binding affinity (41). $ISWI_{FL}$ E257Q was used at 1 μM. Unless stated otherwise, remodeling proceeded for 2 h and was terminated by treatment with 200 mU apyrase (NEB) for 30 min at 30°C. ATP concentration after apyrase depletion was confirmed by ATP assay to be less than 13 μM.

MNase ladder assay. A terminated remodeling reaction mixture sample was supplemented with 1.5 mM $CaCl_2$ (final concentration) and split into aliquots each containing 200 ng DNA. Aliquots were digested with the indicated concentration of MNase (Sigma N5386; diluted in 10 mM Tris [pH 7.4], 0.1 mg/ml bovine serum albumin [BSA] such that 1 to 3 μl of MNase solution was added) for 5 min at 30°C. MNase digests were terminated with EDTA (10 mM final concentration) and treated overnight at 55°C with proteinase K in the presence of 0.5% SDS. After addition of 5 μg *E. coli* tRNA (Sigma) and 10 μg glycogen (Fluka) as carriers, samples were phenol-chloroform extracted and ethanol precipitated. Half of each MNase digest sample was electrophoresed in a 1.5% agarose gel in 1× Tris-acetate-EDTA (TAE) at 100 V for ~2 to 3 h and transferred onto a nylon membrane (Biodyne B; 0.45 μm; Pall Corporation) by capillary blotting, and the membrane was hybridized with radioactively labeled probes directed against the yeast insert (PCR primers for *PHO8* probe, primers 5′-GACGGATCTCGAAGAGATCA-3′ and 5′-CCTGCCATCT GTAATCAACA-3′; for GCY1 probe, 5′-CAGTCGGATGGAGCTCACT TCTATTGGCTTAGGAGC-3′ and 5′-CACTGTGCATTTCTAGAACGA CGAAGACGAGGATTAG-3′), against the pUC19 backbone (primers 5′-TTGCAAGCAGCAGATTACGC-3′ and 5′-TACTTACTCTAGCTTCCC GG-3′), or against the size marker (2-log ladder; NEB). Probes were labeled with [α-^{32}P]dCTP (Hartmann Analytik) using the kit PrimeIt II (Stratagene). Hybridized membranes were exposed to X-ray films (Fuji Super RX). Scanned film images (Epson Perfection V700 scanner) were imported into Adobe Photoshop CS6 and processed by conversion into grayscale format, and linear level adjustment was applied to the entire image. Figure layout was done with Adobe Illustrator CS6.

For samples containing large amounts of $ISWI_{26-648}$, competitor chromatin was added before MNase digestion to avoid interference of bound remodeler with MNase digestion. Here, an aliquot of a terminated remodeling reaction mixture corresponding to 20 ng of pUC19-PHO8 DNA was spiked into a terminated mock (no remodelers) remodeling reaction mixture containing 1 μg SGD chromatin (pUC19-GCY1) followed by MNase digestion and further processing as described above.

For all MNase ladder blots, one representative example of two replicates with independent SDG chromatin is shown, except for Fig. 6 and 7, which were done as one replicate. Nonetheless, both control for the steady state in two different ways and thus reproduce each other.

Purification of remodelers. The pPROEX-HTa-based expression plasmid with the gene encoding *S. cerevisiae* ΔNC-Chd1 (42) was cloned by inserting the ΔNC-Chd1 PCR product (PCR product using primers 5′-GAGCCATGGAAAAGCAATCTACAGTG-3′ and 5′TCCCAAGCTT TCAACTGGGACTCTTTGTATTTAG-3′) via NcoI and HindIII. This adds a His_6-tobacco etch virus (TEV) tag to the N terminus. ΔNC-Chd1 was expressed in *E. coli* Rosetta cells (Novagen). Two liters of induction medium (LB medium containing 0.2 mM isopropyl-β-D-thiogalactopyranoside [IPTG]) was inoculated with cells grown at 37°C and then further cultured overnight at 18°C. Cells were harvested by centrifugation and resuspended in buffer A (50 mM Tris-HCl, pH 7.5, 10% glycerol, 500 mM NaCl, 10 mM imidazole) containing 1 mM phenylmethylsulfonyl fluoride (PMSF), 1× Complete protease inhibitor (Roche), 1× aprotinin, 1× leupeptin, 1× pepstatin, and 1 mM DTT. Cells were lysed using a French press and further disrupted by sonication (Branson digital sonifier; 6 cycles of 10 s on and 10 s off; amplitude, 25%) on ice. After addition of 2 U/ml Benzonase, the lysate was cleared by centrifugation (SS34; 19,000 rpm, 30 min, 4°C) and applied to a HisTrap HP column (GE Healthcare) preequilibrated with 4% buffer B (50 mM Tris, pH 7.5, 10% glycerol, 500 mM NaCl, 400 mM imidazole, 1 mM DTT). After washing with 5 column volumes of 10% buffer B and 1 column volume of 15% buffer B, ΔNC-Chd1 was eluted with a gradient ranging from 15 to 100% buffer B. Fractions containing ΔNC-Chd1 were pooled; dialyzed against 250 mM NaCl, 50 mM Tris-HCl, pH 7.6, 1 mM DTT, and 10% glycerol; and applied to a MonoQ column (GL Amersham) preequilibrated with buffer C (50 mM Tris-HCl, pH 7.6, 10 mM NaCl, 10% glycerol, and 1 mM DTT). After washing with buffer C and elution using a gradient between 10 mM and 1 M NaCl containing buffer C, fractions containing ΔNC-Chd1 were pooled and concentrated (Centricon; Amicon; molecular weight cutoff [MWCO] of 30,000). The final step was size exclusion chromatography on a Superdex200 column (GE Healthcare) (in 50 mM Tris-HCl, pH 7.6, 300 mM NaCl, 10% glycerol, and 1 mM DTT) in order to remove aggregates and contaminating proteins. Peak fractions containing ΔNC-Chd1 were pooled.

pPROEX-HTb-based expression plasmids with genes encoding *Drosophila melanogaster* $ISWI_{FL}$, $ISWI_{FL}$ E257Q, and $ISWI_{26-648}$ were kindly provided by C. Müller (EMBL, Heidelberg, Germany). ISWI derivatives $ISWI_{864::13aa}$ and $ISWI_{871::13aa}$ containing flexible linkers are described in reference 43. All genes were fused N terminally to His_6-TEV tag. Expression and purification were performed as described in reference 44. The His_6-TEV tag was cleaved off by recombinant TEV protease (our own purification) for all ISWI constructs except $ISWI_{26-648}$. Catalytic parameters of $ISWI_{26-648}$ are unaffected by the presence of the tag (41).

D. melanogaster ACF was purified from insect cells by the baculovirus expression system as described previously (45). The integrity of the purified proteins was checked by SDS-PAGE electrophoresis (data not shown).

TEM. Chromatin for transmission electron microscopy (TEM) imaging was prepared by SGD as described above, but BSA and IGEPAL were omitted from the assembly buffer. Chromatin was appropriately diluted in 50 mM NaCl, 10 mM Tris-HCl, pH 7.5, and 1 mM EDTA; adsorbed on glow-discharged Formvar-supported carbon-coated Cu400 TEM grids (Science Services, Munich, Germany); and stained using a 2% aqueous uranyl formate solution containing 25 mM NaOH. Imaging was performed using a Philips CM100 electron microscope operated at 100 kV. Images were acquired using an AMT 4-megapixel charge-coupled device (CCD) camera. Micrograph scale bars were calibrated by imaging two-dimensional (2D) catalase crystals and using the lattice constants as length reference. Imaging was performed at ×28,500 magnification.

Nucleosomes were counted per DNA template in 25 and 19 electron micrographs of high- and low-assembly-degree templates, respectively. Three different persons (C. Lieleg, F. Mueller-Planitz, and P. Korber) counted independently 25 ± 3, 25 ± 3, and 25 ± 4 nucleosomes per 25 high-assembly-degree templates and 11 ± 3, 11 ± 3, and 10 ± 3 nucleosomes per 19 low-assembly-degree templates, respectively (see Fig. 2C).

The absolute number of nucleosomes per linear template for the high assembly degree was somewhat lower, although almost within statistical error, than expected from the topological analysis of the circular templates (25 ± 3 for linear [see Fig. 2C] compared to 31 ± 2 for circular [39] templates). This modest discrepancy was probably due to two reasons. First, circular supercoiled plasmids become reconstituted in SGD with higher efficiency than linear plasmids (46). Second, we omitted BSA from SGD used for electron microscopy as it would clutter the grid and interfere with nucleosome counting. BSA in standard SGD ameliorates the notorious stickiness of histones. So, SGD without BSA may lose histones and produce lower assembly degrees. Nonetheless, results for ISWI-dependent remodeling of BSA-free prepared SGD chromatin with different assembly degrees were equivalent to results with BSA-containing SGD chromatin (data not shown).

Native gel electrophoresis. SGD chromatin corresponding to 100 ng of DNA was mixed with 15 μl low-salt buffer (10 mM Tris-HCl, pH 7.6, 75 mM NaCl, 1 mM EDTA, 1 mM β-mercaptoethanol, and 0.05% IGEPAL-CA630), brought to 1× DNA loading buffer (40% [wt/vol] sucrose, 10 mM Tris-HCl, pH 8.0, 0.25% bromophenol blue), and electrophoresed in an ethidium bromide-free 0.35× Tris-borate-EDTA (TBE), 0.6% agarose gel at 60 V for ~15 h. Southern blot transfer and probe hybridization were done as for the MNase ladder assay.

KpnI accessibility assay. A remodeling reaction mixture sample with pUC19-PHO8 chromatin was incubated for 0 or 4 h (see Fig. 8) and split into aliquots corresponding to 100 ng DNA, and fluorescently labeled 25-mer nucleosomal arrays corresponding to 500 ng DNA were added. After addition of 60 or 150 U KpnI (NEB), remodeling was allowed to proceed at 26°C in the dark until termination with EDTA (25 mM final concentration). DNA was deproteinized by proteinase K, phenol-chloroform extracted, ethanol precipitated, and electrophoresed in an ethidium bromide-free, 1× TAE, 0.9% agarose gel. The fluorescently labeled 25-mer nucleosomal array cleavage products were visualized by Li-Cor Odyssey scanning (green channel, offset = 2). KpnI accessibility was calculated after quantifying the Li-Cor scan using Aida software (Raytest, version 4.27) as intensity of the fragment band after KpnI cleavage/(intensity of the fragment band after KpnI cleavage + intensity of the uncleaved fragment band). Background KpnI accessibility of the SGD-assembled 25-mer nucleosomal arrays was determined in reactions without remodeling enzymes but treated otherwise the same way and subtracted from the KpnI accessibility of remodeler-containing samples. The data were fitted to a single exponential function in Kaleidagraph 4.0. The fit for ACF-generated KpnI accessibility with high KpnI concentration gave unreasonable values for the asymptotic final value such that we used the low KpnI concentration data fit for estimation of the initial slope instead. The fit for Chd1-generated KpnI accessibility after 4 h of incubation gave 36% and 51% of the activity at the 0-h time point for the low and high KpnI concentration, respectively. The KpnI accessibility values shown in Fig. 11 result from a modified assay. Unlabeled, chromatinized pUC19-25-mer corresponding to 200 ng DNA was added to a remodeling reaction mixture sample, after 2 h of remodeling incubation, corresponding to 100 ng DNA pUC19-PHO8. After addition of 150 U KpnI (NEB), remodeling was allowed to proceed at 26°C for 4 h and terminated with EDTA (25 mM final concentration). DNA was purified as described above, and the 25-mer was cut out with XbaI and EcoRI and electrophoresed in an ethidium bromide-containing, 1× TAE, 0.9% agarose gel. The pUC19 backbone fragment was taken as an indicator of total DNA amount, and the KpnI-XbaI fragment was taken as an indicator of fragments generated due to the accessible KpnI site. Band intensities were quantified using Aida software (Raytest, version 4.27) and normalized to fragment size to correct for length-dependent body labeling via ethidium bromide. KpnI accessibility was calculated as intensity of the KpnI-XbaI fragment band/length of KpnI-XbaI fragment/intensity of pUC19 backbone band/length of pUC19 backbone.

Relative quantification of the assembly degree. Unincorporated histones were removed from SGD chromatin via a customized quick spin gel

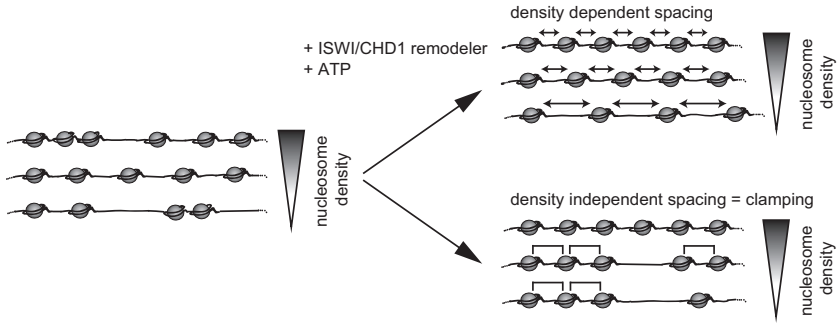

FIG 1 Experimental concept. In classical spacing assays, ISWI- and CHD1-type remodeling enzymes turn irregular and/or tightly spaced nucleosome organizations into regular arrays with wider spacing. In our study, the nucleosome density is varied in order to distinguish if the nucleosomal repeat length scales reciprocally with nucleosome density (double arrows) or is kept rather constant (square brackets). The latter scenario may be the case either because the remodelers actively clamp nucleosomes against each other or because there are attractive direct nucleosome-nucleosome interactions.

filtration column using Sephacryl 300 (Amersham Pharmacia Biotech). The column matrix was equilibrated and blocked with 20 mM HEPES, pH 7.5, 80 mM NaCl, 1.5 mM $MgCl_2$, 0.5 mM EGTA, 2.5 mM DTT, 25 mM $(NH_4)_2SO_4$, and 0.2 mg/ml BSA. Low- and high-assembly-degree chromatin templates, each containing the same amount of DNA, were spun through such columns, the flowthrough was collected, and aliquots were electrophoresed both on a 17.5% SDS-PAGE gel next to the PeqGold protein marker IV (Peqlab) and on a native 0.35× TBE, 0.6% agarose gel for each chromatin type. It was confirmed by treating histones the same way that free histones did not appear in the flowthrough under these conditions. The native gel was blotted and hybridized as described above, and the blots were analyzed by PhosphorImager (Fuji FLA 3000; Fujifilm imaging plate; BAS-MP) using Aida software 4.27 (Raytest). The histone amounts incorporated into the low- and high-assembly-degree chromatin were quantified via the colloidal brilliant blue (Invitrogen)-stained histone bands in the SDS-PAGE gel by determination of area under the curve in line scans over the four histone bands (Aida 4.27). Subsequent normalization of histone amounts as determined via the SDS-PAGE gel to DNA amount determined via the native agarose gel blot assay allowed the comparison of the histone amounts per DNA for both chromatin assembly degrees.

ATP concentration determination. ATP measurements were done using the Enliten ATP assay system bioluminescence detection kit (Promega) according to the manufacturer's protocol and using the Lumat LB9501 luminometer (Berthold). Aliquots from spacing assay reaction mixtures were removed before and after incubation with the remodeling enzyme as well as after apyrase treatment.

Modeling. For our computational simulations, we represent linear 6-kb DNA as a linear lattice with 6,000 sites. Each simulation run consists of two stages: nucleosomes are first placed on the DNA and then iteratively remodeled up to a time t_{max}. To reduce noise, such runs are repeated a large number of times (e.g., 100 times). Time t_{max} is chosen such that the average of the nucleosome distributions at t_{max} of all runs represents the steady state.

For the nucleosome assembly during SGD, we use a coarse-grained approach as our focus is on the remodeling reactions. For the high assembly degree, we place 30 ± 2 nucleosomes on the DNA lattice. This number and the standard deviation are taken from counting nucleosomes by topology (39). For the low assembly degree, we model about half the number of nucleosomes, i.e., place a number of nucleosomes that is drawn from a Poisson distribution with mean 15, which is again compatible with our experimentally determined low assembly degree. To simulate in a coarse-grained way the experimentally observed occurrence of some tight clusters with hardly any linker DNA in SGD chromatin even at low assembly degree, the model deposits nucleosomes as follows. For each nucleosome, a position is first chosen at random respecting steric exclusion of previous ones. If it has a nearest-neighbor nucleosome within a certain range, then it is moved such that the dyad-dyad distance to this neighbor is 150 bp (=tight spacing). The assembly range parameter was chosen to be 500 bp in order to obtain a similar amount of clusters at low assembly degree (gray traces in Fig. 10A) as experimentally observed in MNase ladders. After the initial deposition, nucleosomes are immobile unless they are bound by a remodeler.

The remodeling phase was simulated with an exact event-based Monte Carlo algorithm. In lack of detailed mechanistic knowledge of remodeling reactions, we use a minimal model that can serve as proof-of-principle to show how remodelers could actively generate arrays with constant spacing despite changes in nucleosome density and how this activity could be independent of remodeler concentration. First, remodelers reversibly and iteratively bind to nucleosomes with a certain dissociation constant K_D. Remodeler concentration c is modeled as the ratio of the rates of remodeler binding and unbinding (r_+ and r_-, respectively), such that $K_D = c \cdot r_-/r_+$. Then, bound remodelers can perform sliding reactions which we assume for simplicity to be a random walk with the same sliding rate (r_{slide}) in both directions ($r_{slide} = r_{slide}^{left} = r_{slide}^{right}$ [see Fig. 10B]) with equal probability unless nucleosomes come close together (see below). Each sliding reaction has a step size of 10 bp. Variation of step size had no effect on steady-state nucleosome distributions. Nucleosomes that have a set spacing are attracted to each other, i.e., at these positions the remodeling rate is reduced by the attraction factor A ($r_{slide}^{breakup} = r_{slide}/A$). The reduced rate $r_{slide}^{breakup}$ refers only to terminal nucleosomes that have a neighbor at the set spacing on one side and a long linker on the other side. For the set spacing, we assume a window of 10 bp centered around the experimentally observed spacing of 165 bp. Remodelers cannot slide nucleosomes together more closely than the set spacing.

RESULTS

Experimental strategy. Salt gradient dialysis (SGD) reconstitution generates canonical nucleosomes (47–49). These are distributed over the DNA templates according to DNA sequence intrinsic preferences and maybe nucleosome-nucleosome interactions (31, 50–52). If arrays are formed as detected by MNase ladder analysis, they typically consist of closely packed core particles with hardly any linker DNA (48, 49, 53–56). Incubation with an ISWI- or CHD1-type remodeler increases linker length and extent of array regularity in an ATP-dependent way, which is visualized as more widely spaced and more extensive MNase ladders in agarose gels ("spacing assay"). So far, all published spacing assays involved more or less fully assembled chromatin templates (for examples, see references 23 to 25 and 57). The crucial point of our spacing assays is that we deliberately varied the histone/DNA ratio during SGD to generate chromatin of various assembly degrees (Fig. 1). If

the remodelers simply equalized linker lengths, nucleosome spacing would strongly depend on nucleosome density, i.e., linker lengths should gradually increase with decreasing nucleosome density. Conversely, spacing should not depend on nucleosome density if nucleosomes were clamped together, by either an active packing (31) or a protein ruler (36) mechanism of the remodelers or through attractive nucleosome-nucleosome interactions.

We used three remodelers from two remodeler families and two far-diverged species. From *Drosophila*, we used the recombinant stand-alone ISWI remodeler ATPase, a bona fide remodeling enzyme (22, 41, 58, 59), and the physiological ACF complex consisting of ISWI and the Acf1 subunit (23). As a remodeler from a far-diverged species and different type, we used recombinant monomeric Chd1 from *S. cerevisiae*. Spacing activity for yeast Chd1 was recently demonstrated (57).

Characterization of SGD chromatin templates with high and low assembly degree. Chromatin with various number of nucleosomes per DNA template was prepared by SGD (39). Initially, we used circular plasmids that allowed the determination of the number of nucleosomes per DNA template (= assembly degree) via topological analysis. The assembly degree first increases with increasing histone/DNA ratio but then plateaus before excess histones lead to template aggregation and loss during SGD. The histone/DNA ratio at the onset of the histone titration plateau, as determined for circular templates (39), was used to generate the "high assembly degree." However, in order to avoid different subpopulations due to supercoiled, nicked, and linear forms, we used mainly linear templates. The "low-assembly-degree chromatin" was prepared by using half the amount of histones under otherwise identical conditions.

The difference between the high and low assembly degrees of our chromatin preparations was validated in three ways. First, chromatin of low assembly degree required less MNase to generate comparable digestion degrees and produced less extensive ladders and smears in the lanes than high-assembly-degree templates (see Fig. 3A, lanes 2 to 4 versus 9 to 11; Fig. 3B, lanes 1 to 4 versus 10 to 13; Fig. 3C, lanes 2 to 5 versus 11 to 14; Fig. 4A, lanes 2 to 4 versus 9 to 11; Fig. 4B, lanes 2 to 4 versus 10 to 13 versus 20 to 23; Fig. 5A, lanes 2 to 4 versus 9 to 11; and Fig. 9A, lanes 2 to 4, versus B, lanes 2 to 4). Second, we removed unincorporated histones after SGD by gel filtration and analyzed chromatin aliquots side by side for incorporated histone amounts via SDS-PAGE and Coomassie blue staining and for DNA content by Southern blotting (data not shown). The low-assembly-degree chromatin contained 47% ± 1% of histones per DNA compared to templates of high assembly degree. Third, counting nucleosomes per DNA template in electron micrographs showed that the low assembly degree corresponded to 43% ± 8% of nucleosomes per DNA compared to the high assembly degree (Fig. 2A to C).

The electron micrographs also excluded the possibility that low histone/DNA ratios led to mixed populations of highly and poorly/not assembled templates. This was further confirmed by native gel electrophoresis, which separated all tested assembly degrees and showed only a single band in each case (Fig. 2D and E), arguing for uniform populations. In addition to an uneven intertemplate nucleosome distribution, we also excluded an uneven intratemplate distribution, e.g., between eukaryotic and prokaryotic DNA sequences. Probing the same Southern blots both for the eukaryotic insert (Fig. 3) and for the prokaryotic backbone (data not shown) gave very similar results. Collectively, we confirmed the generation of chromatin templates with substantially different assembly degrees between, but uniform assembly degree within, sample preparations.

Both high- and low-assembly-degree chromatin shows clusters of tightly packed nucleosome core particles. Limited MNase digests of both the low- and high-assembly-degree chromatin showed ladders with very similar repeat lengths of ~150 bp (Fig. 3A, lanes 2 to 4 versus 9 to 11; Fig. 3B, lanes 1 to 4 versus 10 to 13; Fig. 3C, lanes 2 to 5 versus 11 to 14; Fig. 4A, lanes 2 to 4 versus 9 to 11; Fig. 4B, lanes 2 to 4 versus 10 to 13 versus 20 to 23; Fig. 5A, lanes 2 to 4 versus 9 to 11; see Fig. 9A, lanes 2 to 4, versus B, lanes 2 to 4). This corresponds to tightly packed nucleosome core particles with hardly any linker DNA and reproduces much earlier observations that SGD does not generate nucleosome arrays with physiological spacing but rather with very tight spacing, even at lower assembly degrees (48, 49, 53–56). As expected, the ladder extent was much less for the low-assembly-degree templates. Indeed, our and previous electron micrographs show that clusters of tightly packed core particles are rather the exception than the rule for low assembly degrees (Fig. 2) (48, 49, 53, 55). Nonetheless, as suggested by Noll et al. (48), only such tight clusters are abundant enough to consistently yield quantized DNA fragment sizes after MNase digestion that can be seen as distinct ladder bands in electrophoresis. All other nucleosome distributions generate a continuum of DNA fragment sizes, resulting in a smear in the lane background.

We conclude that the more or less extensive MNase ladders generated from SGD chromatin correspond to more or less extensive patches of closely packed core particles, which are well traceable even for our low-assembly-degree chromatin. Such patches are ideal substrates to test if the spacing activity of ISWI- or CHD1-type remodelers will generate spacing that scales reciprocally with nucleosome density. If the latter were true, then the remodelers would generate a substantially larger spacing between nucleosomes in the patches of chromatin with low assembly degree than of chromatin with high assembly degree.

***Drosophila* ISWI and ACF as well as yeast Chd1 remodelers generate similar and constant spacing at low and high assembly degrees.** Incubation of SGD chromatin with the *Drosophila* ISWI remodeler led to more extensive MNase ladders and a noticeably increased spacing of ~160 to 165 bp consistent with previous results (Fig. 3A, lanes 2 to 4 versus 5 to 7 and lanes 9 to 11 versus 12 to 14) (22, 58). This was true for both assembly degrees but more appreciable at higher nucleosome density. Importantly, the repeat length that ISWI established did not increase for the low-assembly-degree chromatin (Fig. 3A, lanes 5 to 7 versus 12 to 14). The same was true for different DNA sequences (Fig. 4A), for circular templates (Fig. 4B), and for the *Drosophila* ACF complex (Fig. 3B) as well as for the yeast Chd1 remodeler (Fig. 3C). The repeat length increase due to ACF and Chd1 was more pronounced than that caused by ISWI and again as previously reported (23, 24, 57). It is notoriously difficult to determine exact DNA fragment sizes from MNase ladders due to band fuzziness, difficult-to-normalize digestion degrees, and electrophoresis variations. Nonetheless, neither ISWI, ACF, nor Chd1 generated substantially wider nucleosome spacing at the low than at the high assembly degree. Moreover, the obtained repeat lengths for the low or high assembly degree remained far away from what the kinetic models would predict (about 400 or 200 bp for complete linker length equalization of the low- or high-assembly-degree templates, respectively)

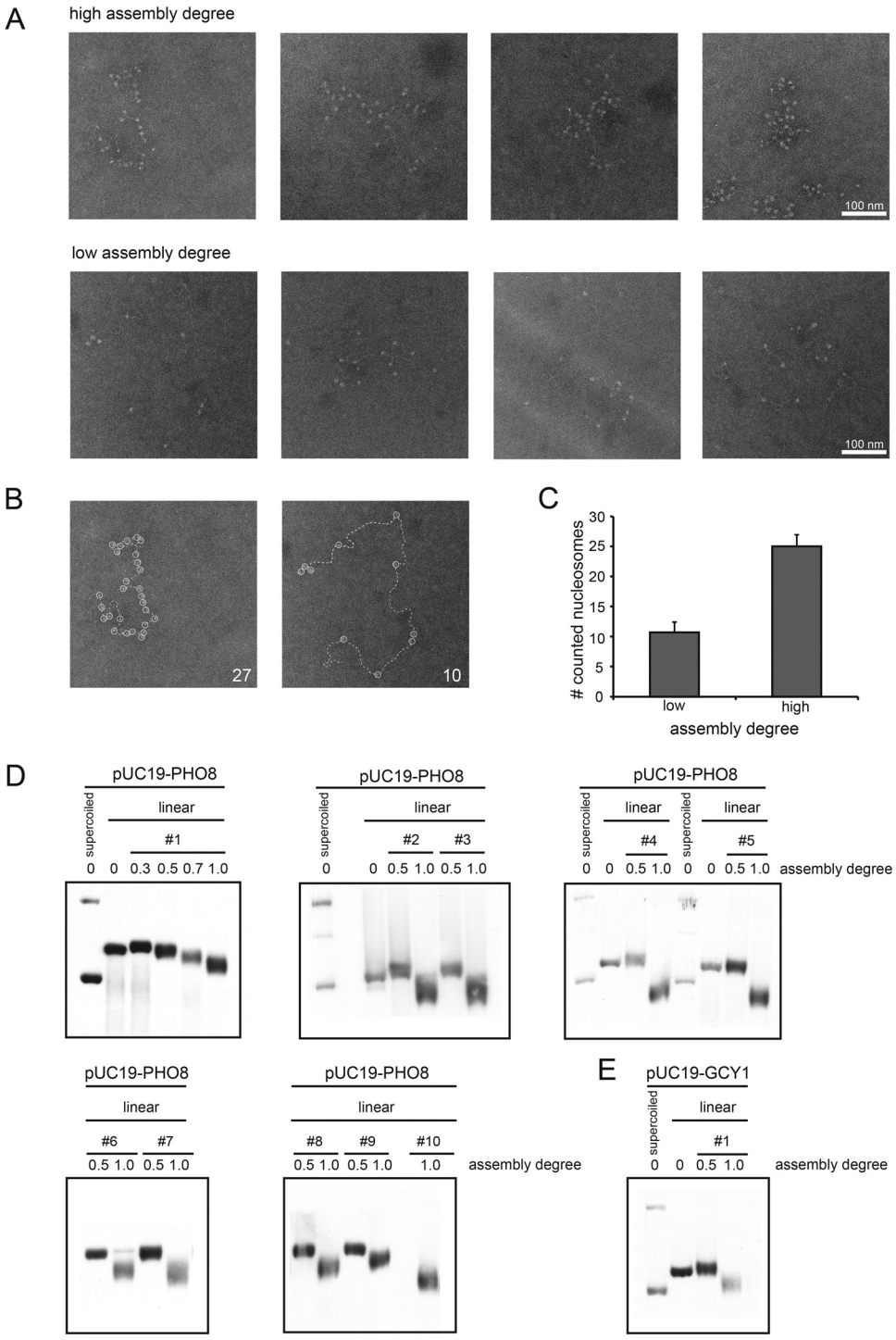

FIG 2 Transmission electron microscopy of SGD chromatin (pUC19-PHO8) and native agarose gel electrophoresis confirmed difference between and uniformity within assembly degrees. (A) Representative TEM images of SGD chromatin with the indicated assembly degree. (B) Interpretive trace of nucleosomes (circles) and DNA (dashed line) in the leftmost TEM images of high- and low-assembly-degree chromatin, respectively, in panel A. Number of counted nucleosomes in lower right corner. (C) Average numbers and standard deviations of nucleosomes for the low- and high-assembly-degree chromatin independently counted by three persons for 25 and 19 micrographs of high and low assembly degree, respectively. (D) Native agarose gel electrophoresis of plasmid pUC19-PHO8 either supercoiled or after linearization with BamHI and SGD reconstitution at the indicated assembly degrees. Numbers 1.0, 0.5, and 0 correspond to high and low assembly degree and no assembly, respectively. The plasmid was detected by Southern blotting and hybridization with a probe directed against the mid-coding region of the yeast *PHO8* gene. Ten different batches of SGD chromatin are shown. Batch 1 was used in Fig. 6A; batch 2 was used in Fig. 5B and 6B; batch 3 was used in Fig. 6C; batch 4 was used in Fig. 3A and B and 7B; batch 5 was used in Fig. 3C, 5A, and 7A; batch 6 was used in panel A; batch 7 was used in Fig. 5C and 7C; batch 8 was used in Fig. 9A and B and 11A; batch 9 was used in Fig. 9B and 11B; batch 10 was used in Fig. 11C. (E) As for panel D but for plasmid pUC19-GCY1 used in Fig. 4A.

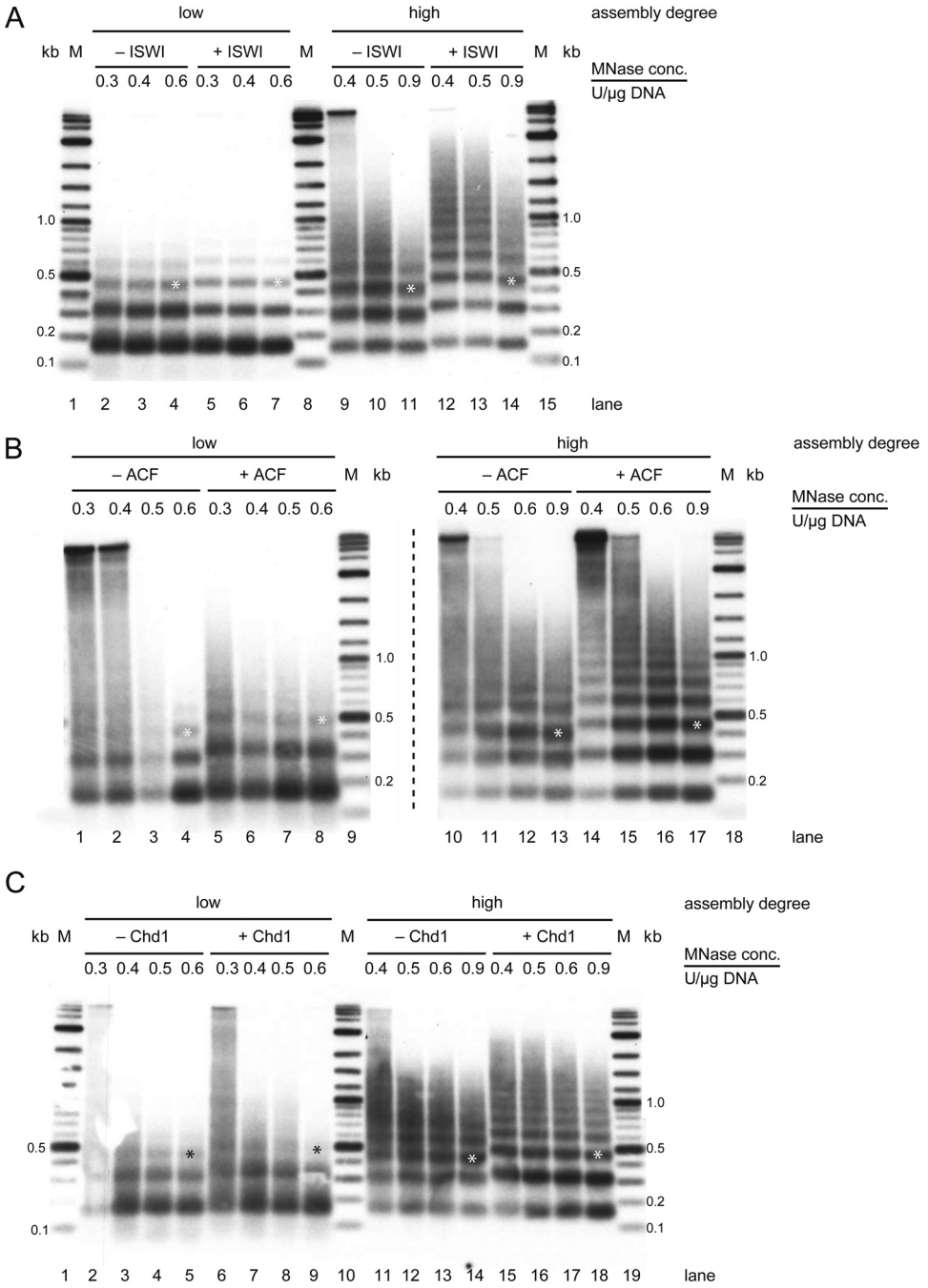

FIG 3 ISWI, ACF, and Chd1 have clamping activity, i.e., they generate very similar and constant nucleosomal repeat lengths regardless of nucleosome density. (A) Limited digests with the indicated MNase concentrations of SGD chromatin (plasmid pUC19-PHO8) at the indicated assembly degrees after incubation with (+ISWI) or without (−ISWI) ISWI remodeler. Asterisks denote the trinucleosomal fragment band. MNase digestion fragments were visualized by Southern blotting and probing against the yeast *PHO8* gene. M, DNA marker (2-log; NEB). (B and C) As for panel A but for the ACF or Chd1 remodeler, respectively.

even though they are within the linker length range that ACF can distinguish (<60 bp [28]). Thus, the lack of substantial increase in spacing at the low relative to that at the high assembly degree is in direct conflict with models in which remodelers simply equalize linker DNA lengths.

Remodeler effects were ATP dependent and not due to remodeler footprints. We ruled out alternative interpretations of our data. First, we excluded the possibility that MNase footprint changes upon remodeler addition were merely due to remodeler binding but not remodeling, as there was no change in nucleosomal repeat length if ATP (Fig. 3) was replaced by the nonhydrolyzable ATP analog AMP-PCP (Fig. 5 and data not shown for a replicate experiment with ISWI and circular templates). In some cases, the nucleosomal fragment bands became somewhat sharper in the presence of remodeler and AMP-PCP, which may stem from remodeler binding to nucleosomes. Importantly, this ATP

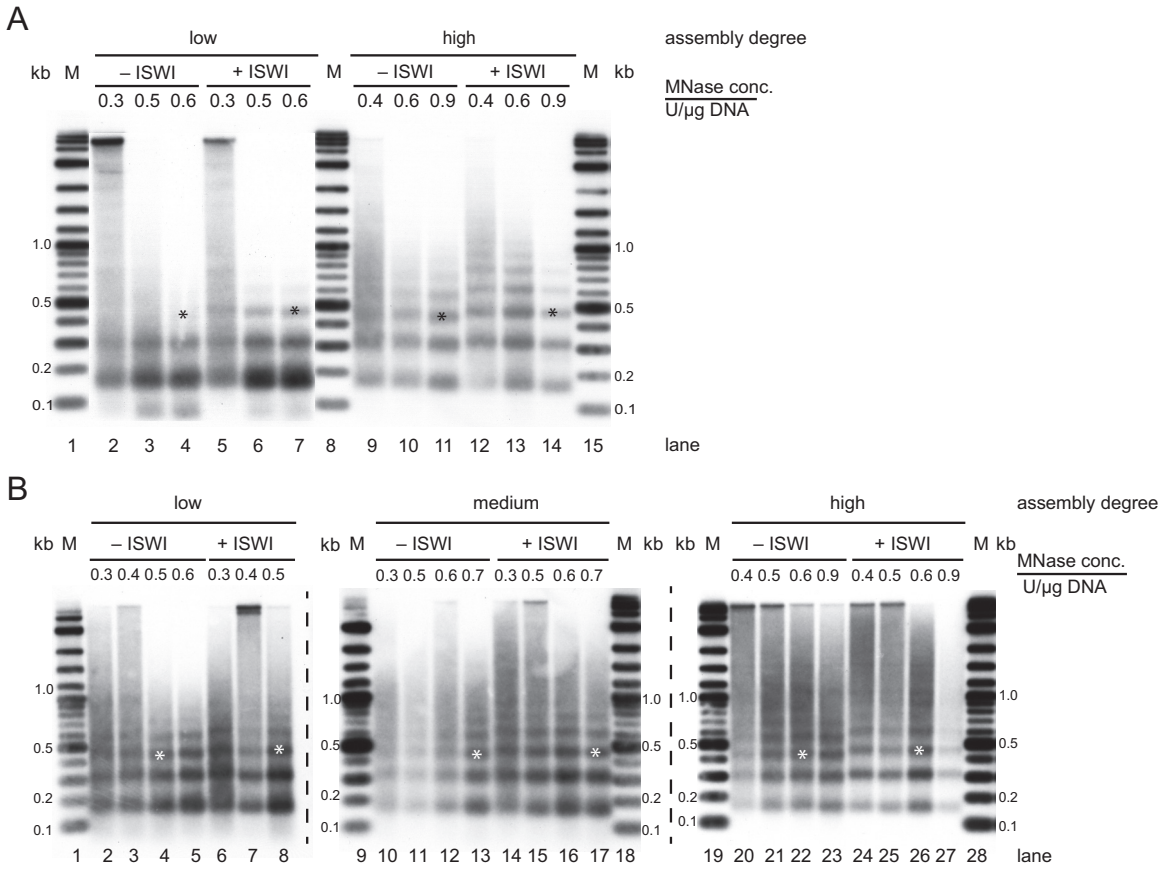

FIG 4 ISWI generated very similar nucleosomal repeat lengths regardless of nucleosome density on linear *GCY1* gene templates and on circular *PHO8* gene templates. (A) As for Fig. 3A but for chromatin assembled on plasmid pUC19-GCY1 and probing against the *GCY1* insert. All samples were electrophoresed in the same gel, but images of different exposure times for lanes 2 to 7 versus 1 and 8 to 15 were combined in this figure using Adobe Illustrator CS6. (B) As for Fig. 3A but for chromatin assembled on circular plasmid pUC19-PHO8 and including an additional "medium" assembly degree with a 0.7-fold histone/DNA ratio compared to the high assembly degree.

dependency also confirmed that all three remodelers were able to remodel these chromatin templates.

The remodeling reactions reached steady state at sufficient remodeler activity and ATP concentrations. Second, we addressed the caveat that nucleosomes were not increasingly spread out at decreasing assembly degrees because we had not reached the steady state of the remodeling reaction. For example, we might have stopped the remodeling reaction too early, the remodelers may have lost all their activity during the assay, or ATP could have been limiting. We ruled out these possibilities. Nucleosome spacing was not substantially changed if the remodeling reaction duration was varied between 2 and 4 h for ISWI (Fig. 6A) and between 0.5 and 4 h for ACF and Chd1 (Fig. 6B and C) or if the remodeler concentration was increased 2- or 3-fold (Fig. 7). ISWI remained fully active and ACF retained 18% and Chd1 retained 44% (Fig. 8C to E) of their activities after 4 h of incubation as measured by restriction enzyme accessibility assay (Fig. 8B). All these activities should have been sufficient to change MNase ladder patterns between the 2- and 4-h time points and even more so between the 0.5- and 2-h time points (Fig. 6) if the reaction had not reached steady state yet. For all three remodelers, ATP concentrations were not substantially depleted during the 4-h time course (at least 60% remaining [data not shown]). Collectively, our results reflect the steady state of remodeling by ISWI, ACF, and Chd1.

Clamping, a novel remodeling activity. Our spacing assays at different nucleosome densities establish that nucleosome spacing is kept constant despite lower nucleosome density. This amounts to a new kind of remodeling activity, the clamping activity. Clamping generates arrays of a constant nucleosome repeat length. If nucleosomes are limiting, these arrays would be interspersed with nucleosome-free regions. Spacing, in the classical sense, would simply equalize linker lengths such that the nucleosome repeat length would vary depending on the nucleosome density (Fig. 1). A comparison of spacings generated at different nucleosome densities amounts to a clamping assay, which is positive if spacing remains constant.

There are at least two different mechanisms that could explain clamping. For the first mechanism, the remodelers would just provide nucleosome dynamics, i.e., "lubricate" nucleosome sliding along DNA, and clamping would be a result of attractive direct nucleosome-nucleosome interactions. We call this the "nucleosome-clamp" mechanism. According to a second mechanism, which we refer to as the "remodeler-clamp" mechanism, the remodeler would interact with and thereby "clamp" two nucleosomes.

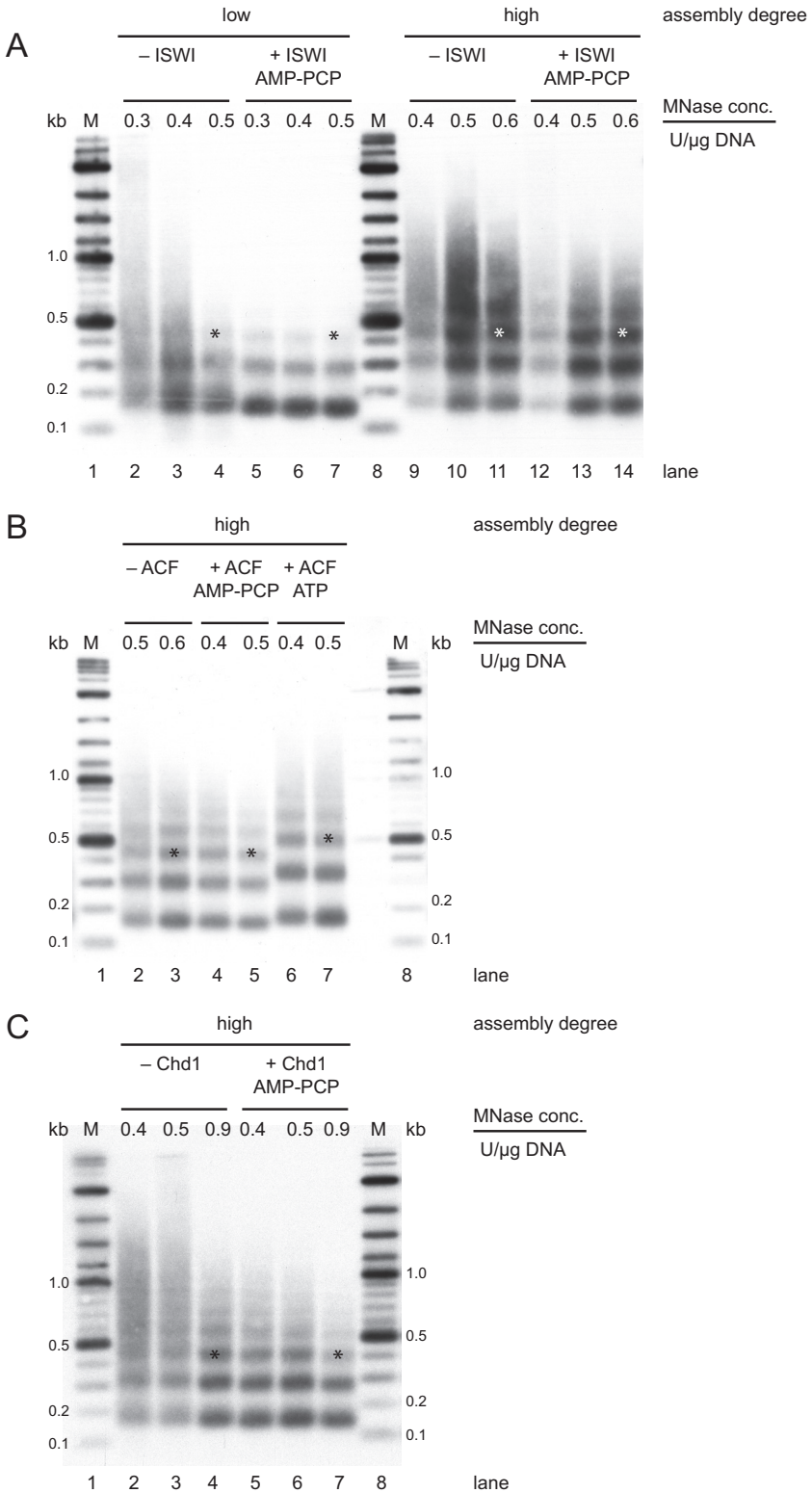

FIG 5 Remodeler-mediated changes in nucleosomal repeat length were ATP dependent and not due to remodeler MNase footprints. (A) As for Fig. 3A but with AMP-PCP instead of ATP. (B) As for Fig. 3B but using ATP or AMP-PCP as indicated. (C) As for Fig. 3C but with AMP-PCP instead of ATP.

We sought to distinguish between these two different clamping mechanisms. If the remodeler needed to remain physically bound to the nucleosomes to clamp them together, one might expect that substoichiometric, catalytic amounts of remodeler should not be able to clamp nucleosomes. We therefore repeated the clamping assay, i.e., a spacing assay at low and high assembly degrees, with substoichiometric amounts of ACF. So far, our remodeling reaction mixtures contained remodelers at roughly stoichiometric

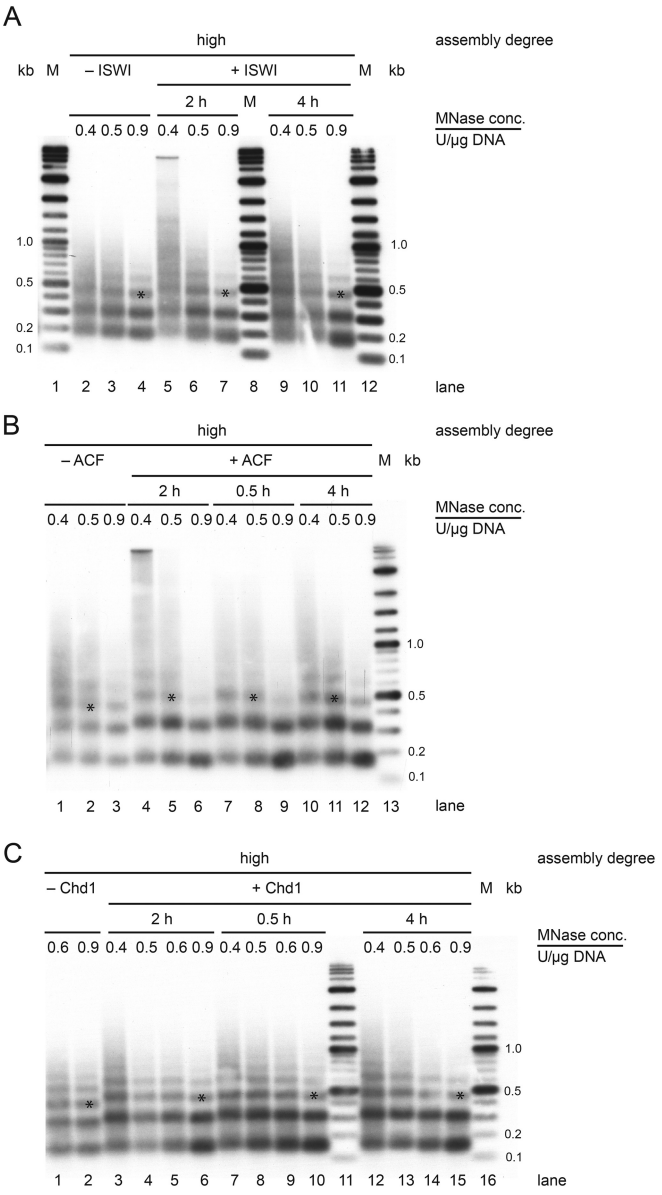

FIG 6 Remodeling reactions by ISWI, ACF, and Chd1 reached steady state. Panels A to C are as for Fig. 3A to C, respectively, but for the indicated time points after addition of remodeler.

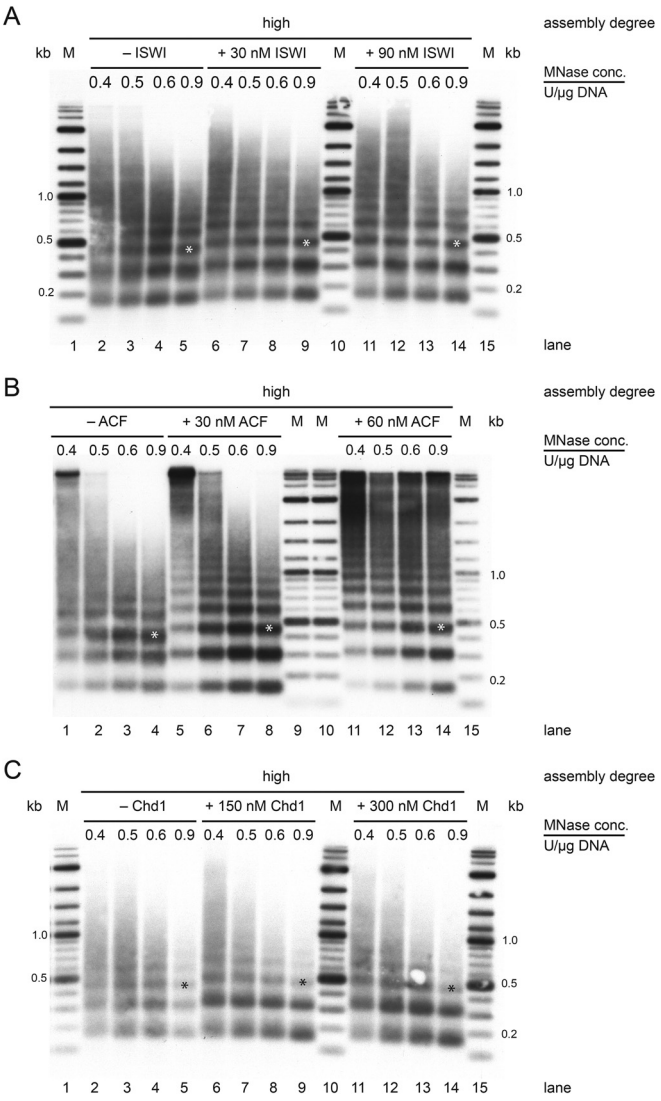

FIG 7 The remodeling outcome remained unaffected when the remodeler concentrations were varied. Panels A to C are as for Fig. 6A to C, respectively, but with two different remodeler concentrations as indicated.

amounts relative to nucleosomes (30 nM ISWI or ACF versus ca. 40/80 nM nucleosomes for low/high assembly degrees, respectively). Now, we used 6 nM ACF versus 40/80 nM nucleosomes, respectively (Fig. 9). At both assembly degrees, we obtained the same spacing of MNase ladders as with the higher, roughly stoichiometric ACF concentrations (30 or 60 nM [Fig. 7B and 9]). Also, the MNase ladder extents were similar. The lower remodeler concentration led to higher digestion degrees at the same MNase concentrations (Fig. 9A, lanes 5 to 7 versus 9 to 17, and B, lanes 5 to 7 versus 10 to 18), but lower MNase concentrations showed again the full MNase ladder extent (Fig. 9B, lanes 25 to 27). The remodeling reaction again reached steady state as there was no further pattern change over time. We conclude that catalytic amounts of ACF can clamp nucleosomes. Note that this result is still consistent with the "clamp" metaphor as it relates only to the final outcome, i.e., constant spacing despite decreased nucleosome density, but need not imply a stoichiometric interaction of the remodeler with the nucleosomes.

Both the nucleosome- and the remodeler-clamp mechanisms can be independent of the remodeler concentration. Indeed, both the remodeler-clamp and the nucleosome-clamp mechanisms are consistent with the observation that catalytic amounts of ACF suffice to clamp nucleosomes, as we show next by a computational approach. We built a minimal model that exhibits clamping activity independent of remodeler concentration (see Materials and Methods) and show that one and the same model can represent both mechanisms.

The model is called "sliding plus attraction" model and posits that remodelers slide nucleosomes along DNA with equal rates in one or the other direction (sliding rate [r_{slide}]) resulting in a one-dimensional random walk. If two nucleosomes come close to each

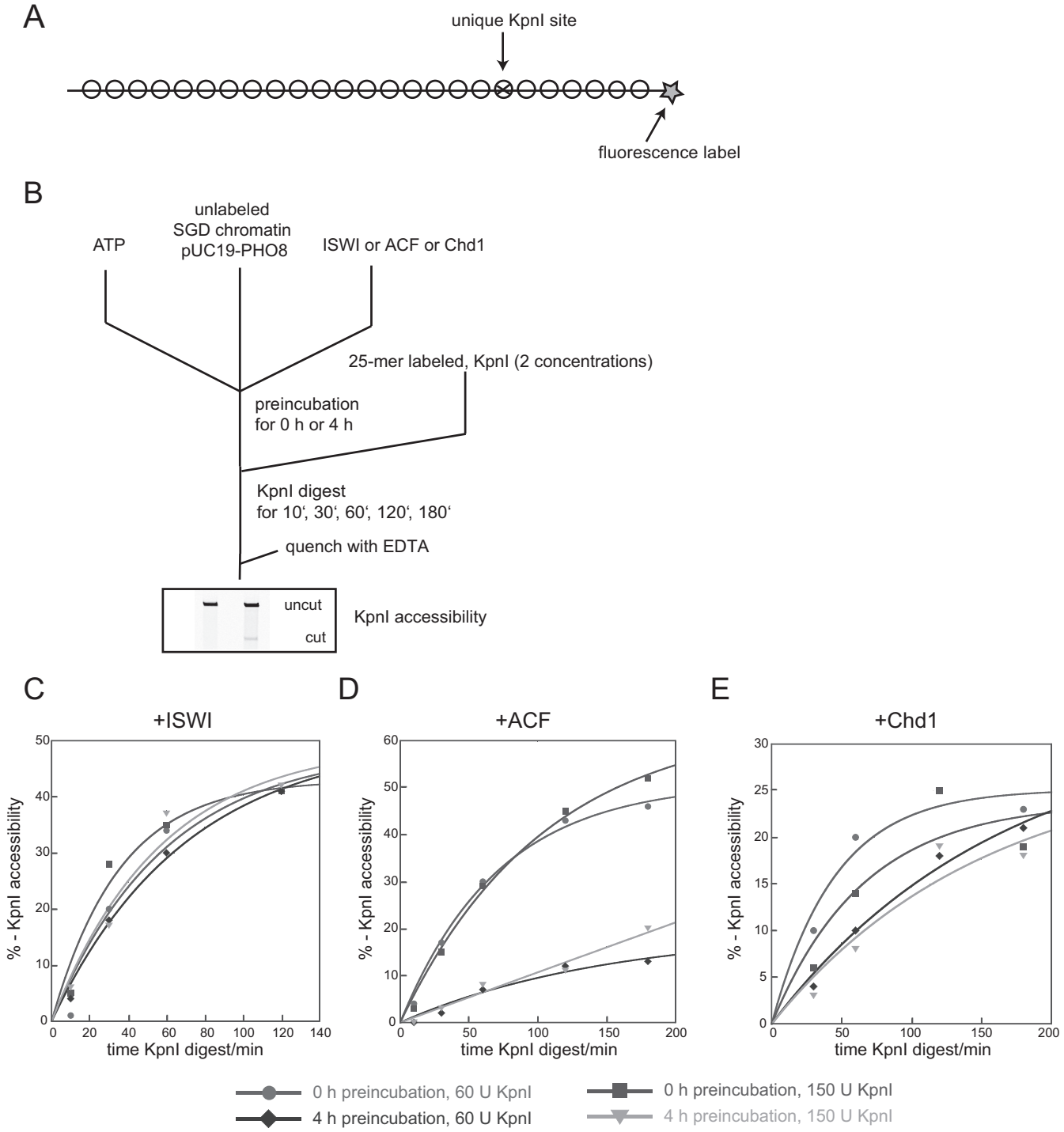

FIG 8 ISWI, ACF, and Chd1 retained sufficient remodeling activity for at least 4 hours to sustain steady-state remodeling. (A) Scheme of nucleosomes assembled on the 25-mer-601-array template with unique KpnI site. (B) Experimental scheme of remodeling assay. SGD chromatin (as in panel A) and either 60 or 150 U of KpnI were added to a spacing assay reaction mixture (see, for example, Fig. 3) after 0 or 4 hours at 26°C. Kinetics of KpnI accessibility in the 19th nucleosome of the 25-mer-601 arrays were used to monitor remodeling activity. (C to E) Kinetics of KpnI accessibility at the indicated preincubation times and KpnI concentrations in the presence of ISWI, ACF, and Chd1, respectively.

other, a functionally attractive nucleosome-nucleosome interaction will generate a set spacing (165 bp) and the interaction energy will lower the chance of the dinucleosome breaking apart in subsequent remodeling cycles. Therefore, arrays are formed because the rate for breaking up arrays ($r_{slide}^{breakup}$) is lower than the rate for bringing nucleosomes together (r_{slide}) by the attraction factor A ($r_{slide}^{breakup} = r_{slide}/A$). Note that all sliding rates are always mediated by the remodeler, which reflects the fact that nucleo-

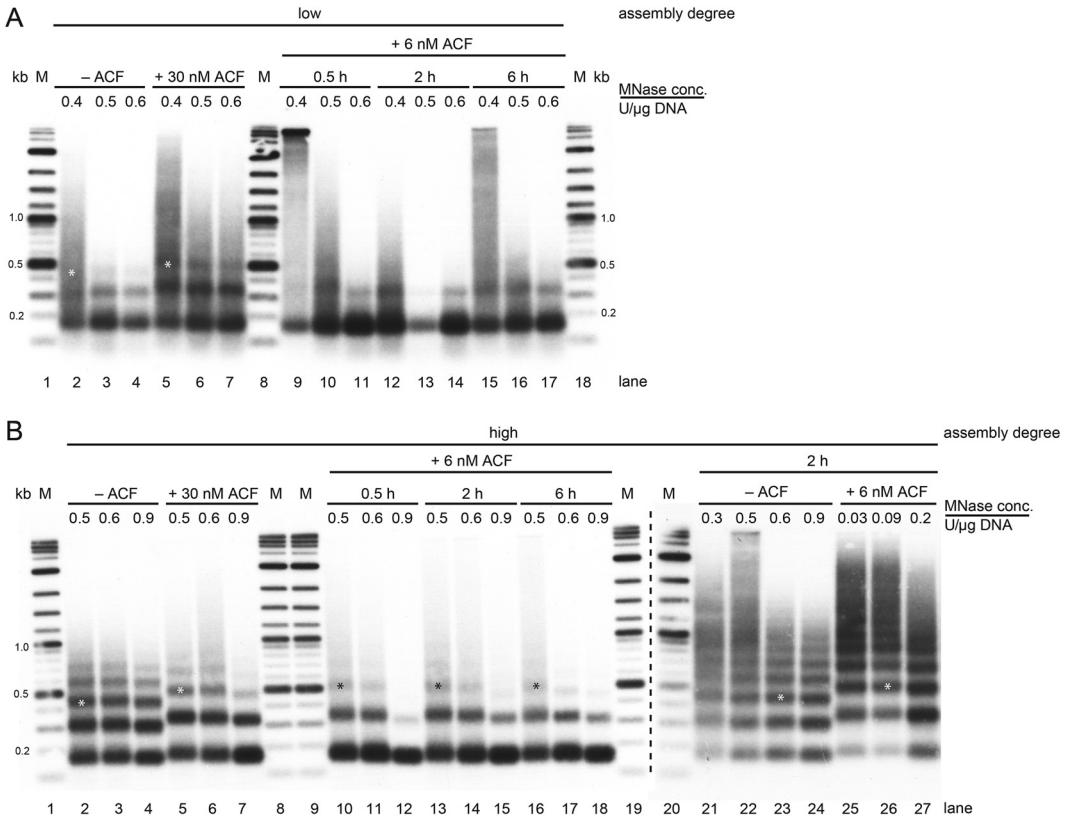

FIG 9 ACF at substoichiometric concentration relative to nucleosomes still generated very similar nucleosomal repeat lengths between neighboring nucleosomes regardless of nucleosome density. Panels are as for Fig. 3B, 6B, and 7B but for the indicated time points and ACF concentrations. The dashed line in panel B separates two independent experiments. Asterisks denote the trinucleosomal fragment band. M, DNA marker (2-log; NEB).

somes are immobile on their own in the absence of remodelers under our rather physiological salt and temperature conditions (60).

Simulations are run until the average distribution of nucleosomes sampled over many templates does not change anymore, i.e., until steady state is reached. To visualize nucleosome distributions, the dyad-to dyad distance distribution is plotted as a histogram (Fig. 10A). Such histograms are related to MNase ladder assays as they plot the occurrence (analogous to band intensity) of distances between nucleosomes (analogous to band position, i.e., fragment length).

The model recapitulates the clamping activity as it transforms tight spacing of the initial conditions into the wider set spacing (shift of peaks in gray versus black traces in Fig. 10A) and keeps this set spacing constant as variation of nucleosome density affects the average array length but not the spacing (Fig. 10A). Array extent is also affected by the attraction factor A: the higher that A is, the longer the arrays. The only exception is infinite A, which leads to kinetic trapping of nucleosomes and prevents long arrays. In the examples shown, array extent is increased only at $A = 100$ for the high assembly degree, but at even higher values for A, array extent will increase in all cases (data not shown). Finally and most important for our argument, the model also recapitulates the results shown in Fig. 9, as nucleosome distributions in steady state do not depend on the remodeler concentration. Only the time until steady state is reached increases with lower remodeler concentrations.

We now show that the attraction factor A may be interpreted in two ways such that this same model can represent either the nucleosome- or the remodeler-clamp mechanism (Fig. 10B). Remodelers can bind to lone nucleosomes in two orientations with equal probability, i.e., equal affinities ($K_D^{\text{left}} = K_D^{\text{right}}$), and the orientation determines the sliding direction. The assumption that the direction of remodeling is linked to the remodeler binding orientation relates well to experimental evidence (36, 61–64). Sliding will bring nucleosomes closely together, and the two mechanisms differ now in the way that the functional nucleosome-nucleosome interaction, represented in the model as the attraction factor A, is generated such that $r_{\text{slide}}^{\text{breakup}}$ becomes lower than r_{slide}. For the nucleosome-clamp mechanism, there is a direct attractive nucleosome-nucleosome interaction that generates the set spacing. This directly counteracts and therefore reduces the rate of sliding nucleosomes apart. For the remodeler-clamp, a remodeler interacts not only with its sliding substrate but also with the neighboring nucleosome if close enough. This additional interaction (IA) generates the set spacing and biases the remodeler in its binding orientation due to the additional interaction energy ($K_D^{\text{left IA}} > K_D^{\text{right}}$). The binding orientation bias directly gives the attraction factor A ($A = K_D^{\text{left IA}}/K_D^{\text{right}}$) and again reduces the rate of sliding nucleosomes apart.

Note that these different interpretations need not be modeled explicitly as they all amount to the same effect, i.e., $r_{\text{slide}}^{\text{breakup}} = r_{\text{slide}}/A$. In molecular terms, both models amount to a functionally attractive interaction between nucleosomes, either directly medi-

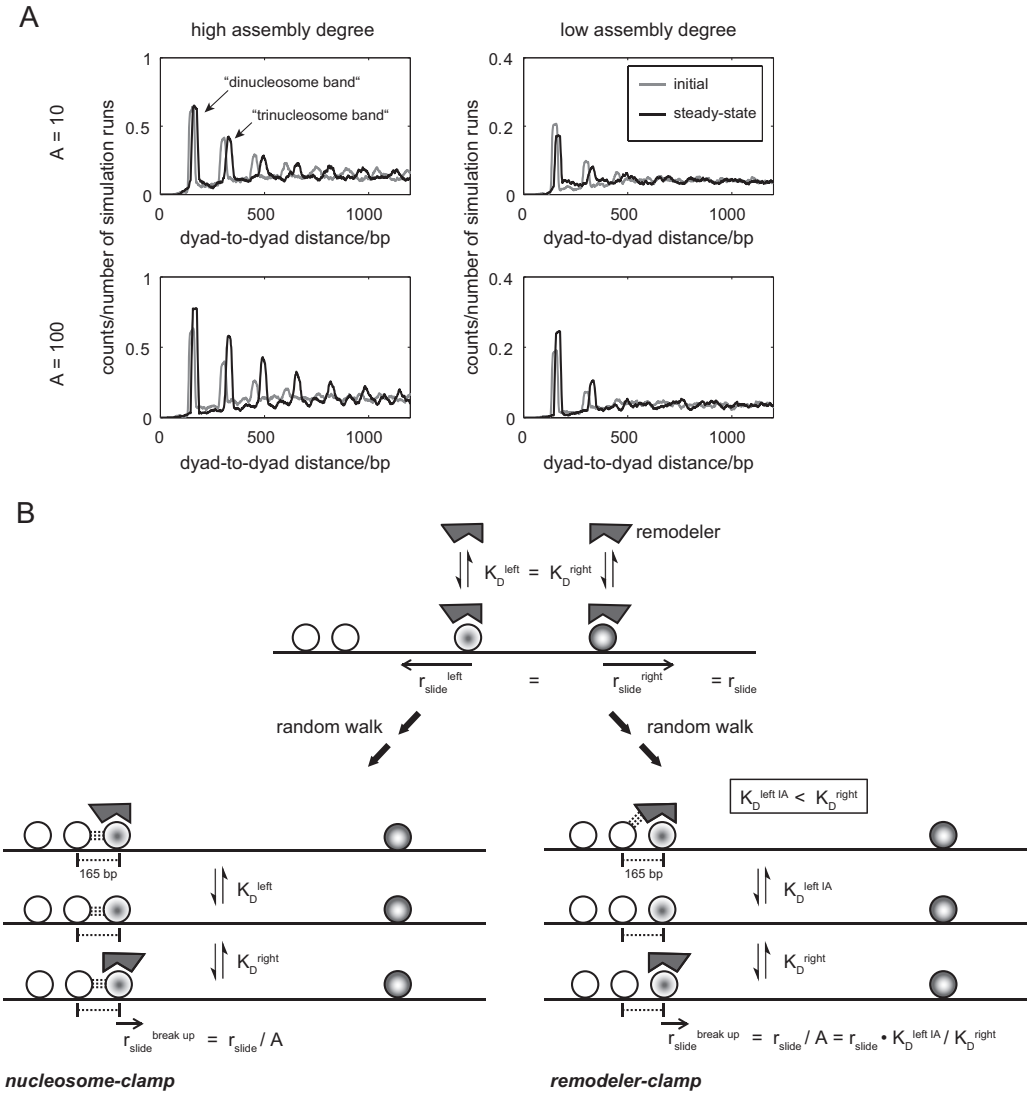

FIG 10 The "sliding plus attraction" model recapitulates the clamping activity and can represent both the nucleosome-clamp and the remodeler-clamp mechanism. (A) Histograms of the initial (gray traces) and steady-state (black traces) distribution of dyad-to-dyad distances after simulation runs of the "sliding plus attraction" model. Such histograms are related to MNase ladder assays as they plot the occurrence (analogous to band intensity) of distances between nucleosomes (analogous to band position, i.e., fragment length). The histogram peaks are analogous to MNase ladder bands as pointed out by arrows. The attraction factor *A* and the assembly degree were varied as indicated. (B) Schematics illustrating the interpretation of the "sliding plus attraction" model as either a nucleosome-clamp or a remodeler-clamp mechanism. For details, see the text. The attractive interaction between nucleosomes or between nucleosome and remodeler is symbolized by a stack of dashed lines. For simplicity, the attractive nucleosome-nucleosome interaction is shown only for the newly added dinucleosome. The butt-ended dashed line labeled "165 bp" merely symbolizes the length of the set spacing but not any other molecular feature. The labeling in the schematics refers to the case that a nucleosome is moved from the right toward another nucleosome or array. Movement from the left is equally possible and would entail converse labeling regarding the superscripts "left" and "right" (e.g., $K_D^{\text{right IA}}$ instead of $K_D^{\text{left IA}}$; IA stands for interaction).

ated by nucleosome-nucleosome or indirectly mediated by nucleosome-remodeler-nucleosome contacts. We explicitly caution that our model serves only as proof-of-principle that both a nucleosome- and a remodeler-clamp mechanism can be independent of remodeler concentration but need not support any claims about the actual molecular mechanism of the clamping activity.

Spacing by ISWI depends on the HSS domain in *cis*. As the remodeler dilution experiment was not conclusive, we sought to uncouple the mere nucleosome sliding activity, which is sufficient for the nucleosome-clamp mechanism, from a putative remodeler-clamp activity. The HAND-SAND-SLIDE (HSS) domain of ISWI-type remodelers was suggested to be important for nucleosome spacing as it can bind and "measure" the length of linker DNA, thereby centering mononucleosomes (28, 61, 65). The HSS domain of *S. cerevisiae* Isw1 was also suggested by mainly structural evidence to be part of a "protein ruler" that sets internucleosomal distances (36). Regarding the mere sliding activity, we previously established that just the ISWI ATPase domain, i.e., the $ISWI_{26-648}$ construct without the HSS and bridge domains, has substantial remodeling activity both in terms of generating accessibility to intranucleosomal restriction sites and in terms of occluding restriction sites in linker regions, i.e., sliding nucleosomes there (41). So, this $ISWI_{26-648}$ construct was a good candidate for a sliding and remodeling activity without spacing activity. Indeed,

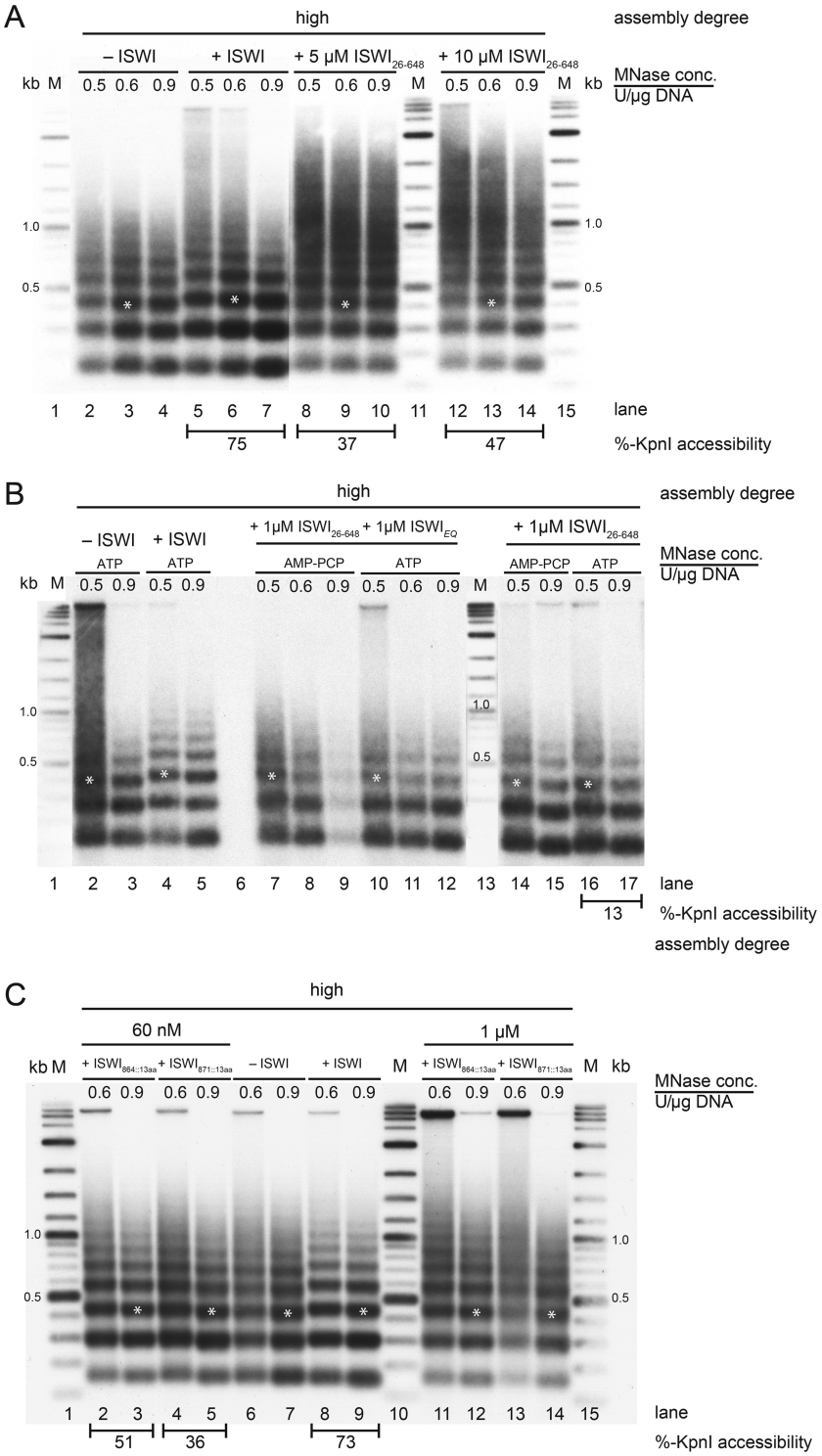

FIG 11 The spacing activity of ISWI remodeler depends on the HAND-SANT-SLIDE domain in *cis*. Panels are as for Fig. 5A and 7A but with the indicated concentrations of the indicated ISWI or ISWI mutant remodelers. Asterisks denote the trinucleosomal fragment band. MNase digestion fragments were visualized by Southern blotting and probing against the yeast *PHO8* gene. M, DNA marker (2-log; NEB). All samples were electrophoresed in the same gel, but images of different exposures for lanes 1 to 7 versus 8 to 15 were combined in panel A and those for lanes 1 and 13 versus 2 to 17 were combined in panel B using Adobe Illustrator CS6. Numbers below the Southern blots reflect remodeling activity after 2 h as determined in the KpnI accessibility assay.

it was negative in our spacing assays (Fig. 11A and B). As positive controls, full-length ISWI increased spacing on the same SGD chromatin templates, and $ISWI_{26-648}$ had remodeling activity under our conditions as judged by spiking in the 25-mer-601-array template and measuring increased KpnI accessibility. The specific activity in the latter assay was lower than that for full-length ISWI as described before (41) and explained by $ISWI_{26-648}$ having lower affinity than full-length ISWI for nucleosomes. But, even at an ~300-fold-higher concentration (up to 10 μM $ISWI_{26-648}$) where $ISWI_{26-648}$ had 63% of ISWI's KpnI accessibility assay activity, there was no spacing activity (Fig. 11A). This argued for a direct contribution of the full-length ISWI remodeler in nucleosome spacing, especially for the HSS domain, and made the nucleosome-clamp model less likely (see Discussion).

If the HSS domain bridged two nucleosomes akin to the protein ruler mechanism (36), we wondered if it could do so in *trans*. However, the combination of $ISWI_{26-648}$ with the ATPase-dead ISWI E257Q mutant did not rescue spacing activity (Fig. 11B), presumably because a linkage in *cis* was necessary.

We showed recently that a rigid connection between HSS and ATPase domains was not necessary for remodeling as would be expected for a power stroke-like energy coupling (43). Nonetheless, it was possible that the connecting length influenced the resulting spacing. So, we tested two different examples of our previously characterized ISWI constructs with 13 amino acids inserted either after position 864 or after position 871 (Fig. 11C). These mutant ISWI remodelers clearly did not generate wider spacing than full-length ISWI. If anything, their spacing activity was a bit less pronounced. The remodeling activity of these ISWI mutants as measured by KpnI accessibility assay after 2 h of incubation was lower than that for full-length ISWI, maybe because the mutant proteins were less stable over time. This residual activity should have been sufficient to allow remodeling, and we confirmed reaching of steady state again by using a higher concentration of the ISWI mutants without change in the resulting patterns.

DISCUSSION

The original length sensor mechanism as proposed for ISWI-type remodelers (28) elegantly explained how ISWI-type remodelers equalize linker lengths on mononucleosomes and how this might be the basis for promoting spacing of nucleosomes in nucleosomal arrays. Here, we tested this mechanism using defined nucleosomal arrays. Surprisingly, our results imply that ISWI and CHD1 remodelers do not equalize linker lengths but rather clamp nucleosomes. We use the term clamping in the sense that two or more nucleosomes are positioned by the remodeler with a fixed spacing regardless of the nucleosome density.

How is clamping achieved mechanistically? Clamping can in principle be accomplished if the nucleosomes that come into contact with each other form direct attractive nucleosome-nucleosome interactions (nucleosome-clamp) or if the remodeler transiently bridges two nucleosomes before it dissociates again (remodeler-clamp). The latter is akin to the protein ruler mechanism proposed for the budding yeast ISW1a complex (36), where structural evidence supports the idea that a remodeler contacts two nucleosomes at the same time and thereby determines spacing. As the protein ruler mechanism was proposed for a specific case, we chose another term to indicate the general mechanism of setting a constant spacing regardless of nucleosome density. Nonetheless, the spacing generated in our assays was in a similar range as the spacing generated by ISW1a in that study.

The strongest argument for our preference for the remodeler-clamp versus the nucleosome-clamp mechanism is that the $ISWI_{26-648}$ remodeler lacking the HSS and bridge domains was negative in our assays even though it has documented sliding activity (41), which should be sufficient for the nucleosome-clamp but not for the remodeler-clamp mechanism.

Surprisingly, $ISWI_{26-648}$ did not generate random nucleosome positions as might be expected and as modeled by us (data not shown) for a mere sliding activity. Perhaps, the thermodynamically preferred nucleosome positions on our arrays are the same as those generated during SGD such that $ISWI_{26-648}$ did not promote net movement of nucleosomes. There is the formal possibility that the $ISWI_{26-648}$ remodeler still had spacing activity but generated such a tight spacing that it could not be distinguished from the tight spacing generated by SGD. Another formal possibility is that $ISWI_{26-648}$ was inactive on the tightly spaced SGD nucleosome arrays but still active on the more widely spaced arrays (repeat length, 197 bp) used for the KpnI accessibility assay.

The nucleosome-clamp mechanism has the advantage of explaining why three different remodelers tested here generate approximately the same spacing. However, the molecular nature of such putative attractive nucleosome-nucleosome interactions remains unclear. It may involve the interaction between the so-called "acidic patch" on histone H2A/H2B and the "basic patch" of the histone H4 tail (66, 67). The nucleosome-clamp mechanism would also entail that the nucleosome-nucleosome interactions leading to array formation were different under our assay conditions from those generated by SGD. This is formally possible as SGD mainly reflects the deposition of the histone H3-histone H4 tetramer at 0.7 to 1 M salt (50).

There is also the formal possibility of a "DNA-clamp" mechanism, i.e., that the nucleosome positions in the arrays are intrinsically encoded by the DNA sequence and will therefore always be occupied as long as a sliding activity is present. However, this mechanism is extremely unlikely as intrinsically DNA-encoded nucleosome positioning preferences have never been found to be strong enough to generate nucleosome arrays *in vitro* with the repeat length reported here (165 bp) but rather always generate tightly packed core particles with hardly any linker (31, 48, 49, 51–53, 55, 56). Also, the DNA intrinsic positioning would have to be strong enough to generate the same nucleosome organization, observed as constant spacing in our case, independent of nucleosome concentration. Finally, our own rehybridization experiments showed generation of the same arrays by the here-tested remodelers also in the prokaryotic vector backbone regions (data not shown). It seems highly unlikely that the same arrays should be intrinsically encoded in prokaryotic as well as eukaryotic sequences.

Collectively, we favor the remodeler-clamp but cannot strictly rule out the nucleosome-clamp mechanism. Clarification of this issue will require further studies.

We note that in our assays the *Drosophila* remodelers did not generate the linker length observed *in vivo* for *Drosophila* (197 bp [68]). Spacing generated in a *Drosophila* embryo extract chromatin assembly system, which is rich in ACF activity (69), depended on ionic strength (70). However, at the ionic strength used by us (>100 mM monovalent cations), the repeat length should be well above 170 bp (70). Apparently, the here-tested remodelers are not sufficient to set the linker length observed *in vivo* or in the context

of *Drosophila* embryo extracts *in vitro*, suggesting that additional factors are needed. Recently, a new embryonic linker histone H1 variant, dBigH1, was discovered in *Drosophila* embryos (71). Lack of dBigH1 decreased the nucleosomal repeat length, making dBigH1 a candidate for setting the physiological spacing in concert with remodelers. The process of transcription was also suggested to influence spacing, both in *S. cerevisiae* (72, 73) and in human cells (8). Further, if large genomic regions are transferred between species, nucleosome spacing along the heterologous DNA was always determined by host cell factors (74, 75), arguing for a strong role of factors beyond histones and DNA in setting nucleosome spacing.

Using a computational approach, Mobius et al. (76) recently modeled that mere inclusion of a dinucleosome clamp in the classical statistical positioning mechanism (29, 30) can account for regular and constant spacing at barriers with fixed +1 nucleosome even at low nucleosome density. This demonstrates that there is no need for a packing mechanism providing directionality against the barrier to explain how arrays with constant spacing are maintained at barriers despite lowered nucleosome density, which was observed *in vitro* and *in vivo* (16, 31–35). Here, we extended these studies and show how a clamping activity maintains arrays with constant spacing also without a barrier.

As proposed before (31), we note that nucleosome density may fluctuate *in vivo* during S phase due to a lag between replication of DNA and reassembly of both DNA copies into nucleosomes. It may be vital that nucleosomes are kept together, especially at important regulatory regions like promoters, even at times of low nucleosome density due to incompletely assembled chromatin. This nucleosome-clamp activity may now be explained through ISWI- and CHD1-type remodeling enzymes.

ACKNOWLEDGMENTS

This work was supported by grants from the German Research Community (DFG) (MU3613/1-1, MU3613/3-1, and SFB1064-A07 to F.M.-P. and SFB/TR5-M6, SFB1064-A04, and KO 2945/1-1 to P.K.) and the Bavarian Research Network for Molecular Biosystems (BioSysNet; to U.G. and P.K.).

We thank Henrike Klinker for providing purified ACF remodeling complex, help with fluorescence labeling, critical reading of the manuscript, and very helpful discussions; Nicola Hepp for cloning pFMP233; Steven Völker for help with Chd1 purification; and Peter Becker for critical comments on the manuscript.

REFERENCES

1. **Kornberg RD, Lorch Y.** 1999. Twenty-five years of the nucleosome, fundamental particle of the eukaryote chromosome. Cell **98:**285–294. http://dx.doi.org/10.1016/S0092-8674(00)81958-3.
2. **Van Holde KE.** 1988. Chromatin, 1st ed. Springer, New York, NY.
3. **Jiang C, Pugh BF.** 2009. Nucleosome positioning and gene regulation: advances through genomics. Nat Rev Genet **10:**161–172. http://dx.doi.org/10.1038/nrg2522.
4. **Mavrich TN, Ioshikhes IP, Venters BJ, Jiang C, Tomsho LP, Qi J, Schuster SC, Albert I, Pugh BF.** 2008. A barrier nucleosome model for statistical positioning of nucleosomes throughout the yeast genome. Genome Res **18:**1073–1083. http://dx.doi.org/10.1101/gr.078261.108.
5. **Struhl K, Segal E.** 2013. Determinants of nucleosome positioning. Nat Struct Mol Biol **20:**267–273. http://dx.doi.org/10.1038/nsmb.2506.
6. **Tsankov AM, Thompson DA, Socha A, Regev A, Rando OJ.** 2010. The role of nucleosome positioning in the evolution of gene regulation. PLoS Biol **8:**e1000414. http://dx.doi.org/10.1371/journal.pbio.1000414.
7. **Lantermann AB, Straub T, Stralfors A, Yuan GC, Ekwall K, Korber P.** 2010. Schizosaccharomyces pombe genome-wide nucleosome mapping reveals positioning mechanisms distinct from those of Saccharomyces cerevisiae. Nat Struct Mol Biol **17:**251–257. http://dx.doi.org/10.1038/nsmb.1741.
8. **Valouev A, Johnson SM, Boyd SD, Smith CL, Fire AZ, Sidow A.** 2011. Determinants of nucleosome organization in primary human cells. Nature **474:**516–520. http://dx.doi.org/10.1038/nature10002.
9. **Berbenetz NM, Nislow C, Brown GW.** 2010. Diversity of eukaryotic DNA replication origins revealed by genome-wide analysis of chromatin structure. PLoS Genet **6:**e1001092. http://dx.doi.org/10.1371/journal.pgen.1001092.
10. **Eaton ML, Galani K, Kang S, Bell SP, MacAlpine DM.** 2010. Conserved nucleosome positioning defines replication origins. Genes Dev **24:**748–753. http://dx.doi.org/10.1101/gad.1913210.
11. **Bassett A, Cooper S, Wu C, Travers A.** 2009. The folding and unfolding of eukaryotic chromatin. Curr Opin Genet Dev **19:**159–165. http://dx.doi.org/10.1016/j.gde.2009.02.010.
12. **Grigoryev SA.** 2012. Nucleosome spacing and chromatin higher-order folding. Nucleus **3:**493–499. http://dx.doi.org/10.4161/nucl.22168.
13. **Korber P, Becker PB.** 2010. Nucleosome dynamics and epigenetic stability. Essays Biochem **48:**63–74. http://dx.doi.org/10.1042/bse0480063.
14. **Routh A, Sandin S, Rhodes D.** 2008. Nucleosome repeat length and linker histone stoichiometry determine chromatin fiber structure. Proc Natl Acad Sci U S A **105:**8872–8877. http://dx.doi.org/10.1073/pnas.0802336105.
15. **Sun FL, Cuaycong MH, Elgin SC.** 2001. Long-range nucleosome ordering is associated with gene silencing in Drosophila melanogaster pericentric heterochromatin. Mol Cell Biol **21:**2867–2879. http://dx.doi.org/10.1128/MCB.21.8.2867-2879.2001.
16. **Hennig BP, Bendrin K, Zhou Y, Fischer T.** 2012. Chd1 chromatin remodelers maintain nucleosome organization and repress cryptic transcription. EMBO Rep **13:**997–1003. http://dx.doi.org/10.1038/embor.2012.146.
17. **Pointner J, Persson J, Prasad P, Norman-Axelsson U, Stralfors A, Khorosjutina O, Krietenstein N, Svensson JP, Ekwall K, Korber P.** 2012. CHD1 remodelers regulate nucleosome spacing in vitro and align nucleosomal arrays over gene coding regions in S. pombe. EMBO J **31:**4388–4403. http://dx.doi.org/10.1038/emboj.2012.289.
18. **Shim YS, Choi Y, Kang K, Cho K, Oh S, Lee J, Grewal SI, Lee D.** 2012. Hrp3 controls nucleosome positioning to suppress non-coding transcription in eu- and heterochromatin. EMBO J **31:**4375–4387. http://dx.doi.org/10.1038/emboj.2012.267.
19. **Smolle M, Venkatesh S, Gogol MM, Li H, Zhang Y, Florens L, Washburn MP, Workman JL.** 2012. Chromatin remodelers Isw1 and Chd1 maintain chromatin structure during transcription by preventing histone exchange. Nat Struct Mol Biol **19:**884–892. http://dx.doi.org/10.1038/nsmb.2312.
20. **Flaus A, Martin DM, Barton GJ, Owen-Hughes T.** 2006. Identification of multiple distinct Snf2 subfamilies with conserved structural motifs. Nucleic Acids Res **34:**2887–2905. http://dx.doi.org/10.1093/nar/gkl295.
21. **Clapier CR, Cairns BR.** 2009. The biology of chromatin remodeling complexes. Annu Rev Biochem **78:**273–304. http://dx.doi.org/10.1146/annurev.biochem.77.062706.153223.
22. **Corona DF, Langst G, Clapier CR, Bonte EJ, Ferrari S, Tamkun JW, Becker PB.** 1999. ISWI is an ATP-dependent nucleosome remodeling factor. Mol Cell **3:**239–245. http://dx.doi.org/10.1016/S1097-2765(00)80314-7.
23. **Ito T, Bulger M, Pazin MJ, Kobayashi R, Kadonaga JT.** 1997. ACF, an ISWI-containing and ATP-utilizing chromatin assembly and remodeling factor. Cell **90:**145–155. http://dx.doi.org/10.1016/S0092-8674(00)80321-9.
24. **Lusser A, Urwin DL, Kadonaga JT.** 2005. Distinct activities of CHD1 and ACF in ATP-dependent chromatin assembly. Nat Struct Mol Biol **12:**160–166. http://dx.doi.org/10.1038/nsmb884.
25. **Varga-Weisz PD, Wilm M, Bonte E, Dumas K, Mann M, Becker PB.** 1997. Chromatin-remodelling factor CHRAC contains the ATPases ISWI and topoisomerase II. Nature **388:**598–602. http://dx.doi.org/10.1038/41587.
26. **Mueller-Planitz F, Klinker H, Becker PB.** 2013. Nucleosome sliding mechanisms: new twists in a looped history. Nat Struct Mol Biol **20:**1026–1032. http://dx.doi.org/10.1038/nsmb.2648.
27. **Narlikar GJ, Sundaramoorthy R, Owen-Hughes T.** 2013. Mechanisms and functions of ATP-dependent chromatin-remodeling enzymes. Cell **154:**490–503. http://dx.doi.org/10.1016/j.cell.2013.07.011.
28. **Yang JG, Madrid TS, Sevastopoulos E, Narlikar GJ.** 2006. The chromatin-remodeling enzyme ACF is an ATP-dependent DNA length sensor that regulates nucleosome spacing. Nat Struct Mol Biol **13:**1078–1083. http://dx.doi.org/10.1038/nsmb1170.

29. **Mobius W, Gerland U.** 2010. Quantitative test of the barrier nucleosome model for statistical positioning of nucleosomes up- and downstream of transcription start sites. PLoS Comput Biol **6**(8):e1000891. http://dx.doi.org/10.1371/journal.pcbi.1000891.
30. **Kornberg RD, Stryer L.** 1988. Statistical distributions of nucleosomes: nonrandom locations by a stochastic mechanism. Nucleic Acids Res **16:** 6677–6690. http://dx.doi.org/10.1093/nar/16.14.6677.
31. **Zhang Z, Wippo CJ, Wal M, Ward E, Korber P, Pugh BF.** 2011. A packing mechanism for nucleosome organization reconstituted across a eukaryotic genome. Science **332:**977–980. http://dx.doi.org/10.1126/science.1200508.
32. **Celona B, Weiner A, Di Felice F, Mancuso FM, Cesarini E, Rossi RL, Gregory L, Baban D, Rossetti G, Grianti P, Pagani M, Bonaldi T, Ragoussis J, Friedman N, Camilloni G, Bianchi ME, Agresti A.** 2011. Substantial histone reduction modulates genomewide nucleosomal occupancy and global transcriptional output. PLoS Biol **9:**e1001086. http://dx.doi.org/10.1371/journal.pbio.1001086.
33. **Gossett AJ, Lieb JD.** 2012. In vivo effects of histone H3 depletion on nucleosome occupancy and position in Saccharomyces cerevisiae. PLoS Genet **8:**e1002771. http://dx.doi.org/10.1371/journal.pgen.1002771.
34. **Hu Z, Chen K, Xia Z, Chavez M, Pal S, Seol JH, Chen CC, Li W, Tyler JK.** 2014. Nucleosome loss leads to global transcriptional up-regulation and genomic instability during yeast aging. Genes Dev **28:**396–408. http://dx.doi.org/10.1101/gad.233221.113.
35. **van Bakel H, Tsui K, Gebbia M, Mnaimneh S, Hughes TR, Nislow C.** 2013. A compendium of nucleosome and transcript profiles reveals determinants of chromatin architecture and transcription. PLoS Genet **9:**e1003479. http://dx.doi.org/10.1371/journal.pgen.1003479.
36. **Yamada K, Frouws TD, Angst B, Fitzgerald DJ, DeLuca C, Schimmele K, Sargent DF, Richmond TJ.** 2011. Structure and mechanism of the chromatin remodelling factor ISW1a. Nature **472:**448–453. http://dx.doi.org/10.1038/nature09947.
37. **Wippo CJ, Israel L, Watanabe S, Hochheimer A, Peterson CL, Korber P.** 2011. The RSC chromatin remodelling enzyme has a unique role in directing the accurate positioning of nucleosomes. EMBO J **30:**1277–1288. http://dx.doi.org/10.1038/emboj.2011.43.
38. **Simon RH, Felsenfeld G.** 1979. A new procedure for purifying histone pairs H2A + H2B and H3 + H4 from chromatin using hydroxylapatite. Nucleic Acids Res **6:**689–696. http://dx.doi.org/10.1093/nar/6.2.689.
39. **Krietenstein N, Wippo CJ, Lieleg C, Korber P.** 2012. Genome-wide in vitro reconstitution of yeast chromatin with in vivo-like nucleosome positioning. Methods Enzymol **513:**205–232. http://dx.doi.org/10.1016/B978-0-12-391938-0.00009-4.
40. **Lowary PT, Widom J.** 1998. New DNA sequence rules for high affinity binding to histone octamer and sequence-directed nucleosome positioning. J Mol Biol **276:**19–42. http://dx.doi.org/10.1006/jmbi.1997.1494.
41. **Mueller-Planitz F, Klinker H, Ludwigsen J, Becker PB.** 2013. The ATPase domain of ISWI is an autonomous nucleosome remodeling machine. Nat Struct Mol Biol **20:**82–89.
42. **Patel A, McKnight JN, Genzor P, Bowman GD.** 2011. Identification of residues in chromodomain helicase DNA-binding protein 1 (Chd1) required for coupling ATP hydrolysis to nucleosome sliding. J Biol Chem **286:**43984–43993. http://dx.doi.org/10.1074/jbc.M111.282970.
43. **Ludwigsen J, Klinker H, Mueller-Planitz F.** 2013. No need for a power stroke in ISWI-mediated nucleosome sliding. EMBO Rep **14:**1092–1097. http://dx.doi.org/10.1038/embor.2013.160.
44. **Forne I, Ludwigsen J, Imhof A, Becker PB, Mueller-Planitz F.** 2012. Probing the conformation of the ISWI ATPase domain with genetically encoded photoreactive crosslinkers and mass spectrometry. Mol Cell Proteomics **11**(4):M111.012088. http://dx.doi.org/10.1074/mcp.M111.012088.
45. **Klinker H, Mueller-Planitz F, Yang R, Forne I, Liu CF, Nordenskiold L, Becker PB.** 2014. ISWI remodelling of physiological chromatin fibres acetylated at lysine 16 of histone H4. PLoS One **9:**e88411. http://dx.doi.org/10.1371/journal.pone.0088411.
46. **Germond JE, Hirt B, Oudet P, Gross-Bellark M, Chambon P.** 1975. Folding of the DNA double helix in chromatin-like structures from simian virus 40. Proc Natl Acad Sci U S A **72:**1843–1847. http://dx.doi.org/10.1073/pnas.72.5.1843.
47. **Lusser A, Kadonaga JT.** 2004. Strategies for the reconstitution of chromatin. Nat Methods **1:**19–26. http://dx.doi.org/10.1038/nmeth709.
48. **Noll M, Zimmer S, Engel A, Dubochet J.** 1980. Self-assembly of single and closely spaced nucleosome core particles. Nucleic Acids Res **8:**21–42. http://dx.doi.org/10.1093/nar/8.1.21.
49. **Spadafora C, Oudet P, Chambon P.** 1978. The same amount of DNA is organized in in vitro-assembled nucleosomes irrespective of the origin of the histones. Nucleic Acids Res **5:**3479–3489. http://dx.doi.org/10.1093/nar/5.10.3479.
50. **Widom J.** 2001. Role of DNA sequence in nucleosome stability and dynamics. Q Rev Biophys **34:**269–324. http://dx.doi.org/10.1017/S0033583501003699.
51. **Zhang Y, Moqtaderi Z, Rattner BP, Euskirchen G, Snyder M, Kadonaga JT, Liu XS, Struhl K.** 2009. Intrinsic histone-DNA interactions are not the major determinant of nucleosome positions in vivo. Nat Struct Mol Biol **16:**847–852. http://dx.doi.org/10.1038/nsmb.1636.
52. **Kaplan N, Moore IK, Fondufe-Mittendorf Y, Gossett AJ, Tillo D, Field Y, LeProust EM, Hughes TR, Lieb JD, Widom J, Segal E.** 2009. The DNA-encoded nucleosome organization of a eukaryotic genome. Nature **458:**362–366. http://dx.doi.org/10.1038/nature07667.
53. **Oudet P, Gross-Bellard M, Chambon P.** 1975. Electron microscopic and biochemical evidence that chromatin structure is a repeating unit. Cell **4:**281–300. http://dx.doi.org/10.1016/0092-8674(75)90149-X.
54. **Patterton HG, von Holt C.** 1993. Negative supercoiling and nucleosome cores. II. The effect of negative supercoiling on the positioning of nucleosome cores in vitro. J Mol Biol **229:**637–655.
55. **Spadafora C, Oudet P, Chambon P.** 1979. Rearrangement of chromatin structure induced by increasing ionic strength and temperature. Eur J Biochem **100:**225–235. http://dx.doi.org/10.1111/j.1432-1033.1979.tb02053.x.
56. **Steinmetz M, Streeck RE, Zachau HG.** 1978. Closely spaced nucleosome cores in reconstituted histone. DNA complexes and histone-H1-depleted chromatin. Eur J Biochem **83:**615–628.
57. **Torigoe SE, Patel A, Khuong MT, Bowman GD, Kadonaga JT.** 2013. ATP-dependent chromatin assembly is functionally distinct from chromatin remodeling. eLife **2:**e00863. http://dx.doi.org/10.7554/eLife.00863.
58. **Clapier CR, Langst G, Corona DF, Becker PB, Nightingale KP.** 2001. Critical role for the histone H4 N terminus in nucleosome remodeling by ISWI. Mol Cell Biol **21:**875–883. http://dx.doi.org/10.1128/MCB.21.3.875-883.2001.
59. **Langst G, Bonte EJ, Corona DF, Becker PB.** 1999. Nucleosome movement by CHRAC and ISWI without disruption or trans-displacement of the histone octamer. Cell **97:**843–852. http://dx.doi.org/10.1016/S0092-8674(00)80797-7.
60. **Korolev N, Vorontsova OV, Nordenskiold L.** 2007. Physicochemical analysis of electrostatic foundation for DNA-protein interactions in chromatin transformations. Prog Biophys Mol Biol **95:**23–49. http://dx.doi.org/10.1016/j.pbiomolbio.2006.11.003.
61. **Dang W, Bartholomew B.** 2007. Domain architecture of the catalytic subunit in the ISW2-nucleosome complex. Mol Cell Biol **27:**8306–8317. http://dx.doi.org/10.1128/MCB.01351-07.
62. **Kagalwala MN, Glaus BJ, Dang W, Zofall M, Bartholomew B.** 2004. Topography of the ISW2-nucleosome complex: insights into nucleosome spacing and chromatin remodeling. EMBO J **23:**2092–2104. http://dx.doi.org/10.1038/sj.emboj.7600220.
63. **McKnight JN, Jenkins KR, Nodelman IM, Escobar T, Bowman GD.** 2011. Extranucleosomal DNA binding directs nucleosome sliding by Chd1. Mol Cell Biol **31:**4746–4759. http://dx.doi.org/10.1128/MCB.05735-11.
64. **Racki LR, Yang JG, Naber N, Partensky PD, Acevedo A, Purcell TJ, Cooke R, Cheng Y, Narlikar GJ.** 2009. The chromatin remodeller ACF acts as a dimeric motor to space nucleosomes. Nature **462:**1016–1021. http://dx.doi.org/10.1038/nature08621.
65. **Ryan DP, Sundaramoorthy R, Martin D, Singh V, Owen-Hughes T.** 2011. The DNA-binding domain of the Chd1 chromatin-remodelling enzyme contains SANT and SLIDE domains. EMBO J **30:**2596–2609. http://dx.doi.org/10.1038/emboj.2011.166.
66. **Pepenella S, Murphy KJ, Hayes JJ.** 2014. Intra- and inter-nucleosome interactions of the core histone tail domains in higher-order chromatin structure. Chromosoma **123:**3–13. http://dx.doi.org/10.1007/s00412-013-0435-8.
67. **Song F, Chen P, Sun D, Wang M, Dong L, Liang D, Xu RM, Zhu P, Li G.** 2014. Cryo-EM study of the chromatin fiber reveals a double helix twisted by tetranucleosomal units. Science **344:**376–380. http://dx.doi.org/10.1126/science.1251413.
68. **Becker PB, Wu C.** 1992. Cell-free system for assembly of transcriptionally repressed chromatin from Drosophila embryos. Mol Cell Biol **12:**2241–2249.

69. **Fyodorov DV, Blower MD, Karpen GH, Kadonaga JT.** 2004. Acf1 confers unique activities to ACF/CHRAC and promotes the formation rather than disruption of chromatin in vivo. Genes Dev **18:**170–183. http://dx.doi.org/10.1101/gad.1139604.
70. **Blank TA, Becker PB.** 1995. Electrostatic mechanism of nucleosome spacing. J Mol Biol **252:**305–313. http://dx.doi.org/10.1006/jmbi.1995.0498.
71. **Perez-Montero S, Carbonell A, Moran T, Vaquero A, Azorin F.** 2013. The embryonic linker histone H1 variant of Drosophila, dBigH1, regulates zygotic genome activation. Dev Cell **26:**578–590. http://dx.doi.org/10.1016/j.devcel.2013.08.011.
72. **Weiner A, Hughes A, Yassour M, Rando OJ, Friedman N.** 2010. High-resolution nucleosome mapping reveals transcription-dependent promoter packaging. Genome Res **20:**90–100. http://dx.doi.org/10.1101/gr.098509.109.
73. **Batta K, Zhang Z, Yen K, Goffman DB, Pugh BF.** 2011. Genome-wide function of H2B ubiquitylation in promoter and genic regions. Genes Dev **25:**2254–2265. http://dx.doi.org/10.1101/gad.177238.111.
74. **Hughes AL, Jin Y, Rando OJ, Struhl K.** 2012. A functional evolutionary approach to identify determinants of nucleosome positioning: a unifying model for establishing the genome-wide pattern. Mol Cell **48:**5–15. http://dx.doi.org/10.1016/j.molcel.2012.07.003.
75. **McManus J, Perry P, Sumner AT, Wright DM, Thomson EJ, Allshire RC, Hastie ND, Bickmore WA.** 1994. Unusual chromosome structure of fission yeast DNA in mouse cells. J Cell Sci **107:**469–486.
76. **Mobius W, Osberg B, Tsankov AM, Rando OJ, Gerland U.** 2013. Toward a unified physical model of nucleosome patterns flanking transcription start sites. Proc Natl Acad Sci U S A **110:**5719–5724. http://dx.doi.org/10.1073/pnas.1214048110.